European Journal of Taxonomy 1090: 1–45
https://doi.org/10.5852/ejt.2026.1090.3321
europeanjournaloftaxonomy.eu
ISSN 2118-9773
2026 · Dadykin I.A. & Pereboev D.D.

Received: 27 February 2026 • *Accepted: 10 June 2026* • *Published: 10 September 2026*

Topic editor: Magalie Castelin • *Section editor: Fabio Stoch* • *Desk editor: Kristiaan Hoedemakers*

Research article

urn:lsid:zoobank.org:pub:7D3D32E7-8523-4255-81E8-9A340FE9B639

Revision of *Drepanothrix* Sars, 1862 (Anomopoda: Macrothricidae), with the description of a new species from East Eurasia and discussion of the genus-specific phylogenetic position and macrothricid paraphyly based on a mitogenome study

Ivan A. DADYKIN[1,*] & Dmitry D. PEREBOEV[2]

[1,2]A.N. Severtsov Institute of Ecology and Evolution of the Russian Academy of Sciences, Leninsky Prospect 33, Moscow 119071, Russia.

[*] Corresponding author: ivan.dadykin@gmail.com
[2] Email: dm.pereboev@gmail.com

Abstract. *Drepanothrix* Sars, 1862 is a monotypic genus of uncertain position within the family Macrothricidae (Cladocera: Anomopoda). Gamogenetic stages of *Drepanothrix* are poorly described despite the importance of their characters for anomopod systematics. *Drepanothrix dentata* (Eurén, 1861) is widespread in the Holarctic, but the conspecificity of its populations from different regions has not yet been proved. This study revises the diversity and phylogenetic position of *Drepanothrix* using morphological criteria, a molecular study based on three genetic loci (COI, 16S rRNA, ITS1), and mitogenomics. Our results show that East Eurasian populations of *Drepanothrix* represent a particular species, *D. asiatica* sp. nov., which differs from *D. dentata* by an absent or reduced dorsal tooth and by the male postabdominal morphology. The study of three gene fragments confirms the differentiation of the two species and assigns Nearctic specimens to a separate clade. Even with new morphological data, the position of *Drepanothrix* within Macrothricidae remains unresolved. The simple structure of limb I inner endite anterior setae, six setae in filtering comb of limb II gnathobase, and limb II exopodite bearing three setae distinguish *Drepanothrix* from the subfamily Macrothricinae to which it was previously attributed. The separate position of *Drepanothrix* is also supported by mitochondrial genomic data, including its mitochondrial genome structure.

Keywords. Cladocera, East Asia, phylogeography, regionalism.

Dadykin I.A. & Pereboev D.D. 2026. Revision of *Drepanothrix* Sars, 1862 (Anomopoda: Macrothricidae), with the description of a new species from East Eurasia and discussion of the genus-specific phylogenetic position and macrothricid paraphyly based on a mitogenome study. *European Journal of Taxonomy* 1090: 1–45. https://doi.org/10.5852/ejt.2026.1090.3321

Introduction

Currently, great efforts are paid to taxonomic and faunistic studies of several macrotaxa within the cladoceran order Anomopoda Sars, 1865 (Branchiopoda Latreille, 1817: Cladocera Latreille, 1829). In recent years, application of DNA barcoding and genomic methods has significantly increased the resolution of taxonomic revisions in different anomopod groups (Kotov *et al*. 2016; Bekker *et al.* 2016; Garibian *et al.* 2021a; Pereboev *et al*. 2025). However, many representatives of Anomopoda still remain unrevised, which is the case for the family Macrothricidae Norman & Brady, 1867. The intricate external morphology of macrothricids has received little scientific attention (Neretina & Kotov 2017), although some of them are rather common in continental water bodies (Smirnov 1992). In the tropics, Macrothricidae sometimes constitute a significant proportion of the fish diet (Growns *et al.* 2020; Quirino *et al.* 2021) and can be used in fish aquaculture (Jiménez-Velásquez *et al.* 2021). The largest genus of Macrothricidae is *Macrothrix* Baird, 1843, while the remaining genera are either monotypic or comprising only a few valid species (Smirnov 1992; Korovchinsky & Kotov 2021).

Drepanothrix Sars, 1862 is one of such monotypic macrothricid genera, which occurs mostly in the temperate zone of the Northern Hemisphere (Smirnov 1992; Korovchinsky & Kotov 2021). The only species of the genus, *D. dentata* (Eurén, 1861), has been reported and illustrated in many monographs (Sars 1862a; Flössner 1972; Fryer 1974; Alonso 1996; etc.) and included in numerous identification guides for Cladocera (Brooks 1959; Scourfield & Harding 1966; Smirnov 1976; Margaritora 1985; Hudec 2010; Rogers *et al.* 2019; Korovchinsky & Kotov 2021). The male morphology of *D. dentata* has received much less attention than that of the parthenogenetic female but was also briefly described by Flössner (1972). Thus, the morphology of *Drepanothrix* seems to be relatively well explored.

However, some data raise the question whether populations of *Drepanothrix* are conspecific across different parts of its range. The genus has a disjunct distribution, which includes West Eurasia, east to northwestern Siberia, East Asia north to China, and North America (Brooks 1959; Smirnov 1976; Korovchinsky & Kotov 2021). To date, *Drepanothrix* has been observed in Central Siberia only once (Yermolayeva & Fetter 2020). According to Frey's noncosmopolitan paradigm (Frey 1982, 1988), East Eurasian and Nearctic populations of *Drepanothrix* could represent separate species, as has already been shown for many anomopods (Kotov *et al.* 2006; Jeong *et al.* 2012; Sinev *et al.* 2020; Dadykin & Pereboev 2025). Moreover, authors of several studies have noted a strong reduction of the dorsal tooth in populations of *Drepanothrix* from the Russian Far East, which is not observed in the European populations (Smirnov 1976; Korovchinsky & Kotov 2021; Dadykin *et al.* 2025). However, the diagnostic significance of this trait is unclear, and previous studies claim that the genus requires further taxonomic revision (Korovchinsky & Kotov 2021; Dadykin *et al.* 2025).

The phylogenetic position of *Drepanothrix* also remains controversial. Based on morphological characters, several authors suggested a subdivision of Macrothricidae into two groups (Dumont & Silva-Briano 1998; Elmoor-Loureiro 2005). In both proposed phylogenies, *Drepanothrix* is considered a congener of *Macrothrix* Baird, 1843, *Bunops* Birge, 1893, *Wlassicsia* Daday, 1904 and *Streblocerus* Sars, 1862, together forming a subfamily Macrothricinae Dumont & Silva-Briano, 1998 (Dumont & Silva-Briano 1998; Dumont & Negrea 2002; Elmoor-Loureiro 2005). However, Dumont & Silva-Briano (1998) noted that the majority of macrothricines have forked anterior setae of thoracic limb I (Fryer's forks) while *Drepanothrix* lacks this synapomorphy and has less modified 'semi-forked' anterior setae. In likely paraphyletic 'non-macrothricines' these setae are unmodified (Dumont & Silva-Briano 1998; Elmoor-Loureiro 2005). Nevertheless, these cladistic analyses have not yet been verified by molecular data, thus the status and phylogenetic position of the groups Macrothricinae and 'non-Macrothricinae' is uncertain.

The present study aims to revise morphological and genetic diversity of *Drepanothrix* in the Northern Hemisphere. Also, we clarify the phylogenetic position of the genus using complete mitochondrial genome data.

Material and methods

Sample collection

We inspected eleven populations of *Drepanothrix* from European and Asian Russia. Samples were collected in 2008–2024 by a throw net with a 50 µm mesh size (Table 1). All analyzed samples were preserved in 96% ethanol and then stored at 4°C. The original specimens were deposited in a working collection of the Laboratory of Aquatic Ecology and Invasions of the A.N. Severtsov Institute of Ecology and Evolution of the Russian Academy of Sciences, Moscow, Russia (IEE AAK M). Also, we examined permanent preparations of *Drepanothrix* stored in the collection of the Zoological Museum of the Moscow State University, Moscow, Russia (MSU, MGU MIs 1178).

Morphological description and processing of images

Individual specimens of *Drepanothrix* were extracted from samples and placed in a glycerol-ethanol mixture drop. Dissections were performed using an Olympus SZ-51 optical binocular microscope (Olympus, Japan) following the technique described by Kotov & Štifter (2006). Line drawings were prepared with an Olympus CX-41 high-power optical microscope equipped with a camera lucida and then inked in Adobe Illustrator 26.0.3 (Adobe Systems Inc., USA) using a graphic tablet Wacom One CTL-672-N (Wacom, Japan). For optical micrography, a LOMO BLM-L optical microscope with an MS-12 digital camera (LOMO-MA, Russia) was used. Each specimen was photographed with a gradual focus shift, with subsequent stacking of the series with Helicon Focus 8 software (Helicon Soft Ltd., Ukraine). All measurements were performed in ImageJ software (Schneider *et al.* 2012) using scale bars calibrated with an eyepiece micrometer for the Olympus CX-41 and LOMO BLM-L optical microscopes.

For scanning electron microscopy, specimens were gradually dehydrated in an ethanol-acetone mixture with increasing acetone concentrations, as follows: 25%, 50%, 75%, 90%, 100%, 100% of acetone. Then the specimens were dried by the critical-point method and dusted with gold. For electron micrography, a TESCAN MIRA scanning electron microscope (TESCAN, Czech Republic) in high vacuum mode was used. Micrographs were processed and illustrations were combined using Adobe Photoshop CC software (Adobe Systems Inc., USA). A map was created in QGIS 3.34.6 software (QGIS Development Team 2026). The Natural Earth vector and raster data (https://www.naturalearthdata.com/) were used as a basemap. The map was visualized using the Lambert Azimuthal Equal Area projection (EPSG:3576).

PCR and sequencing

Genomic DNA was extracted from single individuals using a Wizard Genomic DNA Purification Kit (Promega Corporation, Madison, WI, USA). The individual was dried at room temperature, then placed in the lysis medium (100 µl of Nuclei Lysis Solution, 20 µl of EDTA, and 10 µl of proteinase K), and incubated at 55°C for 18–20 hours. Next, 125 µl of SV Lysis Buffer was added to each specimen. The samples were vortexed, immediately transferred to minicolumns, incubated for 10 min, and then centrifuged at 13000 rcf for 3 min. Then, 650 µl of diluent (Column Wash Solution dissolved according to the original protocol) was added to each sample, with two rounds of centrifugation (3 min at 13000 rcf and 2 min at 13000 rcf). The minicolumns were then transferred to a new microtube. The DNA was eluted in three steps: for each round, 30 µl of distilled water (pre-heated to 55°C) was added to a minicolumn, incubated for 10 min at room temperature and centrifuged for 3 min at 13000 rcf. The extracted DNA was stored at -20°C.

We amplified two mitochondrial gene fragments, Folmer's cytochrome oxidase I (COI) and 16S rRNA, using newly designed primer pairs: simo_folmer_F (5'-TCRACTAATCATAAGGATATTGG-3') / simo_lf_R (5'-CCTCTYTCATGACTAATAATATG-3') for Folmer's *COI* and 16Sdp1f (5'-GACTGTGCTAAGGTAGCATAATC-3') / 16Sdp1r (5'-CCGGTTTGAACTCAGATCATGT-3') for 16S rRNA. For PCR, the Encyclo PCR kit was used (Eurogene, Russia). All PCRs, except for ITS1

Table 1. List of the studied localities and samples of *Drepanothrix* Sars, 1862.

Locality number	Collection number	Region and country	Locality	Latitude	Longitude	Date	Collector
1	AAK M–2642	Murmansk Area, Russia	Lake Lovozero	68°3.890′ N	35°15.908′ E	10 August 2013	A.N. Reshetnikov
2	AAK M–2852 AAK M–7018	Moscow Area, Russia	Lake Glubokoe	55°45.217′ N	36°30.250′ E	29 October 2014, 18 September 2021	A.A. Kotov, P.G. Garibian
3	AAK M–8715	Tver Area, Russia	Abandoned peat mining near Merilovo Village	56°52.811′ N	36°48.571′ E	22 September 2024	I.A. Dadykin
4	AAK M–7069	Khabarovskii Krai, Russia	Small lake at eastern shore of the Nikolay Bay	53°54.000′ N	138°41.770′ E	27 August 2021	O. Shpak
5	AAK M–0864	Sakhalin Area, Russia	Sphagnal lake near Pokrovka Village	47°19.234′ N	142°42.432′ E	15 September 2008	A.A. Kotov, N.M. Korovchinsky
6	AAK M–6526	Sakhalin Area, Russia	Simushir Island, a small sphagnal bog	47°7.088′ N	152°16.452′ E	22 July 2019	M.O. Ivanova
7	AAK M–6527 AAK 2006–011 ZIN 55223	Sakhalin Area, Russia	Simushir Island, a small sphagnal bog	47°6.040′ N	152°14.262′ E	22 July 2019	M.O. Ivanova
8	AAK M–3027 AAK 2026–012 MGU MI–287 MGU MI–288 MGU MI–289 ZIN 55222	Kamchatskii Krai, Russia	Small drying thermokarst lake in the Kronotsky Nature Reserve	54°13.921′ N	160°9.696′ E	21 August 2014	E.I. Bekker, F.V. Kazansky
9	AAK M–3029	Kamchatskii Krai, Russia	Small thermokarst lake in the Kronotsky Nature Reserve	54°14.162′ N	160°9.756′ E	21 August 2014	E.I. Bekker, F.V. Kazansky
10	AAK M–3028	Kamchatskii Krai, Russia	Small thermokarst lake in the Kronotsky Nature Reserve	54°13.967′ N	160°9.810′ E	21 August 2014	E.I. Bekker, F.V. Kazansky
11	AAK M–7655	Kamchatskii Krai, Russia	Karaginsky Island, a small slightly brackish lake	58°33.621′ N	163°29.034′ E	16 July 2022	I.A. Dadykin
12	AAK M–7720	Kamchatskii Krai, Russia	Karaginsky Island, a small lake with muddy sediment	58°58.135′ N	163°53.052′ E	5 August 2022	I.A. Dadykin
13	AAK M–6493	Kamchatskii Krai, Russia	Bering Island, a small lake in tundra near Nikolskoe Village	55°13.291′ N	166°0.654′ E	28 September 2020	O. Krylovich, E. Kuzmicheva, O. Smyshlyaeva
14	MGU MIs 1178	Chukotskii Autonomous Region, Russia	A puddle in the vicinity of Anadyr River	65°0.000′ N	171°0.000′ E	7 August 1972	N.N. Smirnov
15*	–	Ontario, Canada	Eel Lake	44°33.786′ N	77°26.790′ W	29 May 2016	M. Elias-Gutierrez, P. Hebert, M. Valdez-Moreno

* A population of *Drepanothrix* with only molecular data available.

amplification, were performed in a 25 µl reaction volume (5 µl of HS-Encyclo Buffer, 14 µl of distilled water, 2 µl of forward primer, 2 µl of reverse primer, and 2 µl of DNA template). The PCR conditions for *COI* were as follows: 95°C for 5 min; 5 cycles: 95°C for 30 s, 48°C for 50 s, 72°C for 1 min; 34 cycles: 95°C for 30 s, 50°C for 50 s, 72°C for 1 min; 72°C for 5 min. The PCR conditions for 16S rRNA were: 95°C for 5 min; 38 cycles: 94°C for 30 s, 59°C for 45 s, 72°C for 1 min; 72°C for 5 min. Additionally, we amplified the nuclear ITS1 fragment for several specimens using newly designed primers: ITS1dp1f (5'-GGTGAACCTGCGGAAGGATC-3') and ITS1dp1r (5'-GTGATCCACCGTTCAGGGTC-3'). PCRs for ITS1 amplification were performed in a 25 µl reaction volume (5 µl of HS-Encyclo Buffer, 15 µl of distilled water, 2 µl of ITS1dp1f, 2 µl of ITS1dp1r, and 1 µl of DNA template). The PCR conditions for ITS1 were: 95°C for 5 min; 38 cycles: 94°C for 30 s, 63°C for 45 s, 72°C for 1 min; 72°C for 5 min. The size of all PCR products was verified by 1% agarose gel electrophoresis.

The PCR products were purified using the GentaPure Cleanup kit according to the protocol (GenTerra, Russia). Two-directional Sanger sequencing was performed by Syntol Ltd. (Russia). Sequence processing and contig construction were performed in the CodonCode Aligner ver. 11.0.2 (CodonCode Corporation, USA). The resulting contigs were verified by BLASTn comparisons (Boratyn *et al*. 2013). Additional sequences were obtained from the NCBI GenBank database (Sayers *et al*. 2019). Then, all contigs were aligned by Unipro UGENE ver. 52.1 (Okonechnikov *et al*. 2012) using the MAFFT tool (Katoh & Standley 2013).

Single- and multigene analyses

For phylogenetic reconstructions, the IQ-TREE ver. 3.0.1 standalone version was employed (Wong *et al*. 2026). Phylograms were constructed by the maximum likelihood method based on sequences from *COI*, *16S rRNA*, and homozygous *ITS1* gene fragments. The best nucleotide substitution models were detected automatically (Kalyaanamoorthy *et al.* 2017). Branch support was assessed from the 1000 replicates of the SH-aLRT test (Guindon *et al*. 2010) and 10 000 replicates of the ultrafast bootstrap (Hoang *et al*. 2018). The phylograms were visualized with FigTree ver. 1.4.4 (http://tree.bio.ed.ac.uk/software/figtree/). TCS haplotype networks (Clement *et al*. 2002) were constructed and visualized for the *COI* and *16S rRNA* gene fragments using PopArt 1.7 (Leigh *et al*. 2015). The *16S rDNA* sequences with large gaps were excluded from the final alignment prior to the network construction. The list of sequences included in the analysis is presented in Supp. file 2: Table S1.

Mitogenomic analyses

To assemble mitochondrial genomes, we obtained short-read whole-genome sequencing (WGS) data for *Drepanothrix dentata* from Lake Glubokoe, Moscow Area, Russia (AAK M-7018). As no verified mitogenomic data on the Macrothricidae family was available in public databases, we used original genomic data for *Macrothrix triserialis* Brady, 1886 from Bến Tre Province, Vietnam (9°48.268′ N, 106°36.732′ E) as comparative material. For both *D. dentata* and *M. triserialis*, we isolated the DNA from individual parthenogenetic females fixed in 96% ethanol. Genomic DNA was extracted into 50 µL of eluent solution using the QIAamp Micro Kit (Qiagen, Hilden, Germany) according to the manufacturer's protocol. Library preparation and WGS ("Animal & Plant WGRS" on the DNBSEQ Platform, at least 12 Gbp as paired reads of 100 bp) were performed by BGI Genomics Co., Ltd. (China).

The raw reads were filtered by fastp ver. 0.23.4 (Chen 2023), and then we assembled and annotated mitochondrial genomes as described earlier (Pereboev *et al*. 2025) using GetOrganelle ver. 1.7.7.1 (Jin *et al*. 2020 and references therein) and Mitoz ver. 3.6 (Meng *et al*. 2019 and references therein). Structure of the putative control region was verified by Sanger sequencing. We used a newly designed primer pair drepa12s_e (5'-ACCCCTGATACACAAGGTAC-3') / drepa16s_b (5'-ACATATCGCCCGTCACTC-3'). The PCR conditions were as follows: 95°C for 5 min; 39 cycles: 95°C for 30 s, 52°C for 50 s, 72°C for 1 min; 72°C for 5 min. DNA purification and sequencing were performed as stated above.

Gene map visualization was created using the Proksee web-service (Grant *et al*. 2023). Obtained data were combined with other publicly available mitogenomes of Anomopoda (Supp. file 2: Table S2). Both rRNA genes and all codon positions for every protein-coding gene were used. Individual genes were aligned using MAFFT ver. 7.525 (Katoh & Standley 2013) with the L-INS-i algorithm. Gap-rich regions were removed by trimAl ver. 1.4.rev15 (Capella-Gutiérrez *et al*. 2009) with the '-automated1' option. We used IQ-TREE ver. 2.2.6 with automatic model selection (Kalyaanamoorthy *et al*. 2017) and the greedy strategy of automatic partitioning (Chernomor *et al*. 2016) to reconstruct phylogenetic trees with 1000 ultrafast bootstrap replicates (Hoang *et al*. 2018) and 1000 SH-aLRT replicates (Guindon *et al*. 2010). The final mitogenome dataset was composed of 25 taxa, including 5 partitions with 12 946 total sites. The tree was rooted with *Podonevadne trigona* (Sars, 1897) (Onychopoda Sars, 1865: Podonidae Mordukhai-Boltovskoi, 1968) as an outgroup.

Abbreviations and terms

The terminology for morphological structures generally follows Dadykin & Pereboev (2025), and numbering of thoracic limb I endites follows Neretina & Kotov (2017). Setae of the outer limb portion or exopodite are labeled with Latin letters (a–g), setae of the inner portion with Arabic numerals (1–9 for posterior setae and 1'–9' for anterior setae), and gnathobase posterior elements with Greek letters (α–ε) (Dadykin & Pereboev 2025).

In the descriptions, we use the following abbreviations:
IDL = inner distal lobe of the limb I
ms = male accessory seta of the antenna I
ODL = outer distal lobe of the limb I
SDL = subdistal lobe of the limb I

The abbreviations used in figures are decoded in the respective figure captions.

The following institutional abbreviations are used throughout the text:
IEE = working collection, Laboratory of Aquatic Communities and Invasions, A.N. Severtsov Institute of Ecology and Evolution of the Russian Academy of Sciences, Moscow, Russia
MSU = Zoological Museum, Lomonosov Moscow State University, Moscow, Russia (sample numbers MGU MI#)
ZIN = Zoological Museum, St Petersburg State University, Saint Petersburg, Russia

Results

Taxonomy

Class Branchiopoda Latreille, 1817
Order Anomopoda Sars, 1865
Family Macrothricidae Norman & Brady, 1867

Genus ***Drepanothrix*** Sars, 1862

Drepanothrix Sars, 1862a: 156–158 (type species *Drepanothrix dentata* (Eurén, 1861: 118), by subsequent designation by Sars (1862a: 156–158).

Diagnosis

The genus *Drepanothrix* can be diagnosed by an ovoid body with a well-developed keel in parthenogenetic females and males but reduced in gamogenetic females. Valves are ornamented with thin polygons. Dorsal valve margin forms a dorsal tooth which can be either well developed or reduced.

Dorsal organ is small and conical. Gut forms double loops. Female postabdomen is subrectangular in lateral view, the preanal angle is shifted towards the posterior end of postabdomen; the dorsal keel of the postabdomen is absent. Preanal margin of postabdomen is armed with transverse rows of long setulae; anal margin of postabdomen bears clusters of spines and setulae. Antenna I bears 9 terminal aesthetascs, each ending with two hooks. Formula of antenna II swimming setae is 0–0–0–3/1–1–3, spine formula is 0–1–0–1/0–0–1. Inner endites of thoracic limb I bear setulose or denticulate anterior setae lacking forks. Thoracic limb II exopodite has three setae. Thoracic limb V is strongly reduced, includes an epipodite, an exopodite bearing a single seta, and an inner portion with three setae. Gamogenetic female has an angulate dorsal margin of the carapace. Ephippium is transparent, lacks clear ventral border and specific sculpture, and contains two resting eggs. Male is small, male valves form a ventral outgrowth with enlarged marginal armature. Male postabdomen is weakly or strongly modified as compared to that of female, gonopore occupies a subdistal position. Male antenna I bears an additional seta on the anterior edge. Male antenna II bears two additional setae on basipodite distal end. Male thoracic limb I forms a subdistal lobe with two setae.

Drepanothrix dentata (Eurén, 1861)
Figs 1–5

Acantholeberis dentata Eurén, 1861: 118.

Drepanothrix setigera – Sars 1862a: 156–158.
Drepanothrix hamata – Sars 1862b: 300. — Norman & Brady 1867: 13–14, pl. XXII figs 6–7.
Drepanothrix dentata – P.E. Müller 1867: 138–139, pl. II fig. 13. — Lilljeborg 1900: 368–372, tab. LVII, figs 3–16. — Keilhack 1909: 70, figs 165–166. — Herr 1913: 419–431, figs 4–18; 1917: 82–84, figs 36a, 37. — Berg 1929–1930: 66–68, pl. IV figs 1–5. — Parenzan 1932: 140–141, tav. 18, figs 8–9. — Hollwedel 1953: 56, fig. 16. — Srámek-Hušek *et al.* 1962: 306. — Manuilova 1964: 195–197, fig. 89. — Flössner 1972: 257–259, figs 121–122. — Fryer 1974: 183–190, figs 50–55. — Smirnov 1976: 163–166, figs 149–152; 1992: 119–121, figs 604–509. — Margaritora 1985: 166–188, fig. 76. — Alonso 1996: 230–234, figs 102–103. — Dumont & Silva-Briano 1998: pls 1, 3–4. — Kotov 2006: fig. 3c–d; 2013: figs 28e, 81в, 94а–б, 101а–б. — Alekseev & Tsalolikhin 2010: 222, pl. 129 fig. 1, pl. 130 figs 5–7. — Hudec 2010: 232–233, fig. 64. — Rogers *et al.* 2019: pl. 16.2.24 figs a–c. — Korovchinsky & Kotov 2021: 232–234, pl. 68 figs 1–4.

Diagnosis

Dorsal valve margin of parthenogenetic female and male forms a well-developed dorsal tooth. Postabdomen of male is weakly modified relative to that of female. Preanal angle is roughly right, shifted towards anal opening. Postabdominal claw is short and stout (length : width = 2.7–3.2); the outer surface of the claw bears two clusters of spinulae not forming pectens.

Type material

The type specimens of this species are likely lost.

Material examined

RUSSIA • 2 parthenogenetic ♀♀; Murmansk Area, Lake Lovozero; 68°3.890′ N, 35°15.908′ E; 10 Aug. 2013; A.N. Reshetnikov leg.; IEE, IEE AAK M–2642 • 22 parthenogenetic ♀♀, 10 ephippial ♀♀, 8 ♂♂; Moscow Area, Lake Glubokoe, littoral zone with sandy sediment and *Fragmites*; 55°45.217′ N, 36°30.250′ E; 29 Oct. 2014; A.A. Kotov leg.; IEE, IEE AAK M–2852 • 10 parthenogenetic ♀♀, 4 ephippial ♀♀, 7 ♂♂; same data as for preceding; 18 Sep. 2021; P.G. Garibian leg.; IEE, IEE AAK M–7018 • 2 parthenogenetic ♀♀; Tver Area, abandoned peat mining pond near Merilovo

Village, littoral zone with *Fragmites*; 56°52.811′ N, 36°48.571′ E; 22 Sep. 2024; I.A. Dadykin leg.; IEE, IEE AAK M–8715.

Type locality

"Sjön Barken" in southern Sweden (coordinates of the lake center are 57°12.81′ N, 12°37.86′ E).

Description

Parthenogenetic female

Body. Length is 0.32–0.9 mm. Body ovoid in lateral view (length : height = 0.66–0.75), flattened laterally (width : length = 0.35–0.45), with a well-developed dorsal keel in both head and valves (Figs 1A–B, 2A, 3A). Headshield is ornamented with elongate cells. Carapace has a rather fine sculpture of irregular polygons (Figs 1A, 2A). Dorsal valve margin forms a well-developed dorsal tooth (Figs 1A, D, 2A, 3B). Ventral valve margin is evenly convex, armed with transverse cuticular flanges and long feathered setae (Fig. 1A). Posterodorsal valve angle is not pronounced (Figs 1A, 2A, 3A).

Head. Large, body 2 × as long as head, strongly flattened laterally (HL/HW = 1.3–1.5), lacking prelabral outgrowths (Figs 1A, 2A, 3A). Posterior head portion forms a cervical groove reaching a mandibular joint laterally (Figs 1A, 2A–B). Dorsal organ is located at posterior edge of head keel; the dorsal organ consists of a conical projection and cuticular ring (Fig. 2B). Lateral head pores are absent. Frontal pore is small, horseshoe-shaped, located at anterior head margin closely to bases of antennae I (Fig. 2I). Ocellus is smaller than the compound eye, located closely to the base of antenna I (Figs 1A, 3A, 4A).

Thorax. Relatively short, smooth, bearing five pairs of appendages. Gut is coiled, forming several double loops (Figs 1A–B, 3A). Abdomen is short, smooth, lacks projections (Figs 1A, 3A).

Postabdomen. Short and subquadrangular, 0.2 × as long as the body, 1.3–1.4 × as long as high (Figs 1C, 2E). Anal opening is terminal. The preanal margin of postabdomen is armed with transverse rows of long setulae. The anal margin of postabdomen bears clusters of spines and setulae. Postabdominal claws are short and stout, 3.0–3.3 × as long as wide (Fig. 1C). The lateral margin of the postabdominal claw is armed with two clusters of spinulae that do not form pectens (Fig. 1C, see also Figs 1J–K, 2K–L). Basal spine of the claw is short (Fig. 1C). Postabdominal seta is inserted on a low projection (Fig. 1C), 0.6–0.7 × as long as the postabdomen, bisegmented. Basal seta portion bears a single row of sparse long setulae anteriorly; distal seta portion exceeds the basal one in length, distal portion bears three rows of long sparse setulae (Fig. 1A).

Labrum. Long, lacking labral keel, often bearing two denticles on the anterior edge (Fig. 4H–I). Lateral cuticular flange borders the posterior margin of the labrum; a row of long setulae is located along the flange (Fig. 4H). Labrum apex is triangular to blunt triangular (Fig. 4H–I). Labral outgrowth is short, conical or rounded, covered with setulae (Fig. 4H–I).

Antenna I. Attached to the anterodorsal head angle (Figs 1A, 3A, 4A). Antenna I is long, strongly flattened laterally, bent at ~120° in anterior view, slightly S-shaped in lateral view. Antenna I anterior edge is armed with clusters of spinulae (Fig. 4A–B). Antenna I bears a basal sensory seta (Fig. 4A–B), and nine terminal aesthetascs subequal in size, each terminating in two hooks (Fig. 10C).

Antenna II. 0.9–1.1 × as long as body length. Coxal portion of the antenna II bears two sensory setae, proximal one is 1.7 × as long as distal one (Fig. 4C). Basipodite has a long distal burrowing spine (1.5 × as long as exopodite segment 1) on the outer side, and a distal sensory seta on the inner side. Exopodite is four-segmented: exopodal segment 1 is short, segments 2 and 3 are subequal in length, 1.8–2.0 × as long as segment 1; segment 4 is 1.5–1.6 × as long as segment 3 (Fig. 4C). Endopodite is three-segmented:

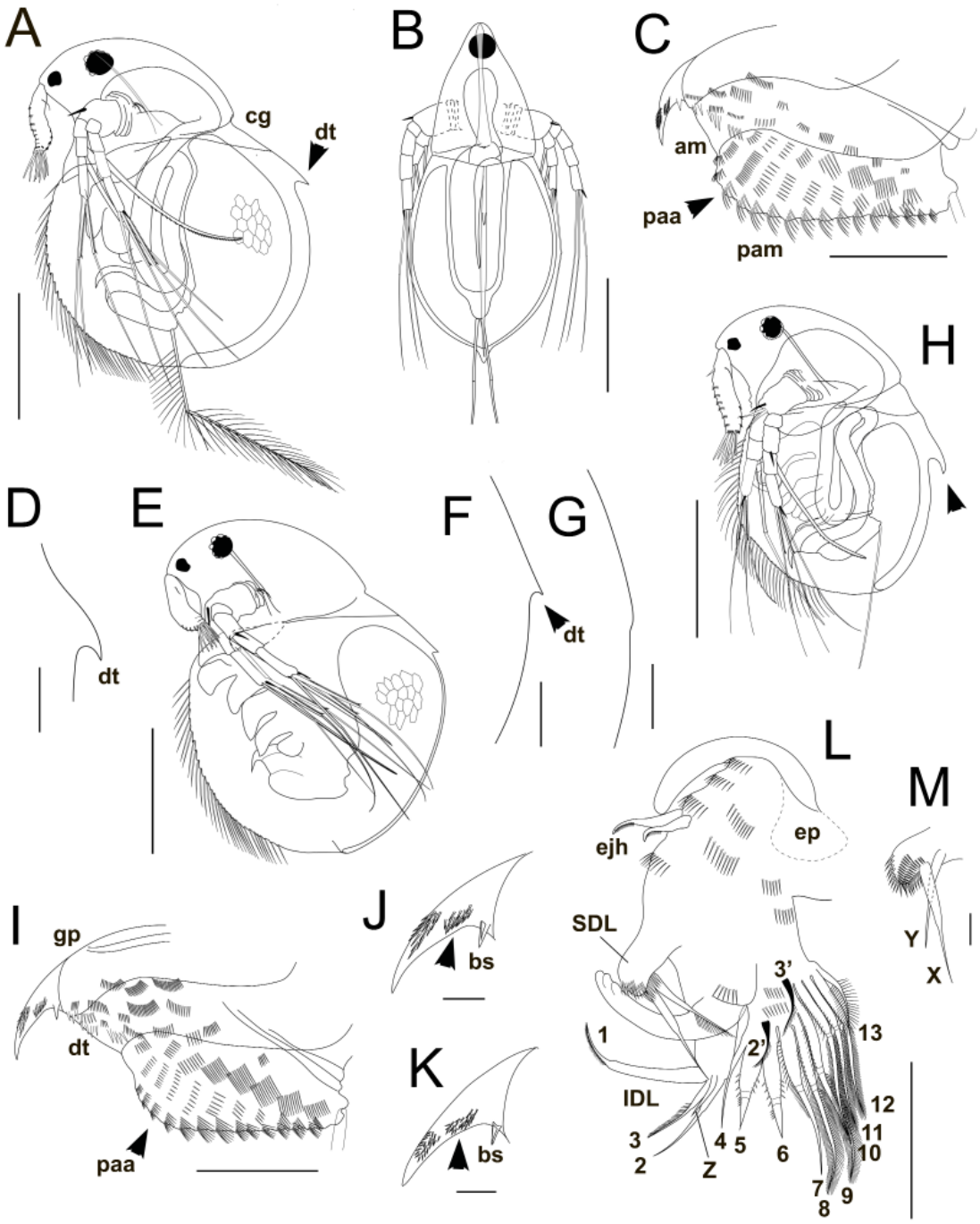

Fig. 1. *Drepanothrix dentata* (Eurén, 1861) from Lake Glubokoe, Moscow Area, Russia (IEE AAK M–7018). **A–D**. Adult parthenogenetic, female. **A**. Lateral view. **B**. Dorsal view. **C**. Postabdomen, lateral view. **D**. Dorsal tooth in lateral view. **E–G**. Ephippial female. **E**. Lateral view. **F–G**. Variability of dorsal tooth. **H–M**. Adult male. **H**. Lateral view. **I**. Postabdomen in lateral view. **J–K**. Postabdominal claw in outer views. **L**. Thoracic limb I in anterior view, maxillary process is not shown. **M**. Subdistal lobe of the thoracic limb I. Abbreviations: am = anal margin of postabdomen; bs = basal spine of postabdominal claw; cg = cervical groove; dt = dorsal tooth; ejh = ejector hooks of thoracic limb I; ep = epipodite; gp = gonopore; IDL = inner distal lobe of thoracic limb I; paa = preanal angle of postabdomen; pam = preanal margin of postabdomen; SDL = subdistal lobe of thoracic limb I. For seta labeling, see Material and methods. Scale bars: A–B, E, H = 200 µm. C–D, F–G, I, L = 50 µm. J–K, M = 10 µm.

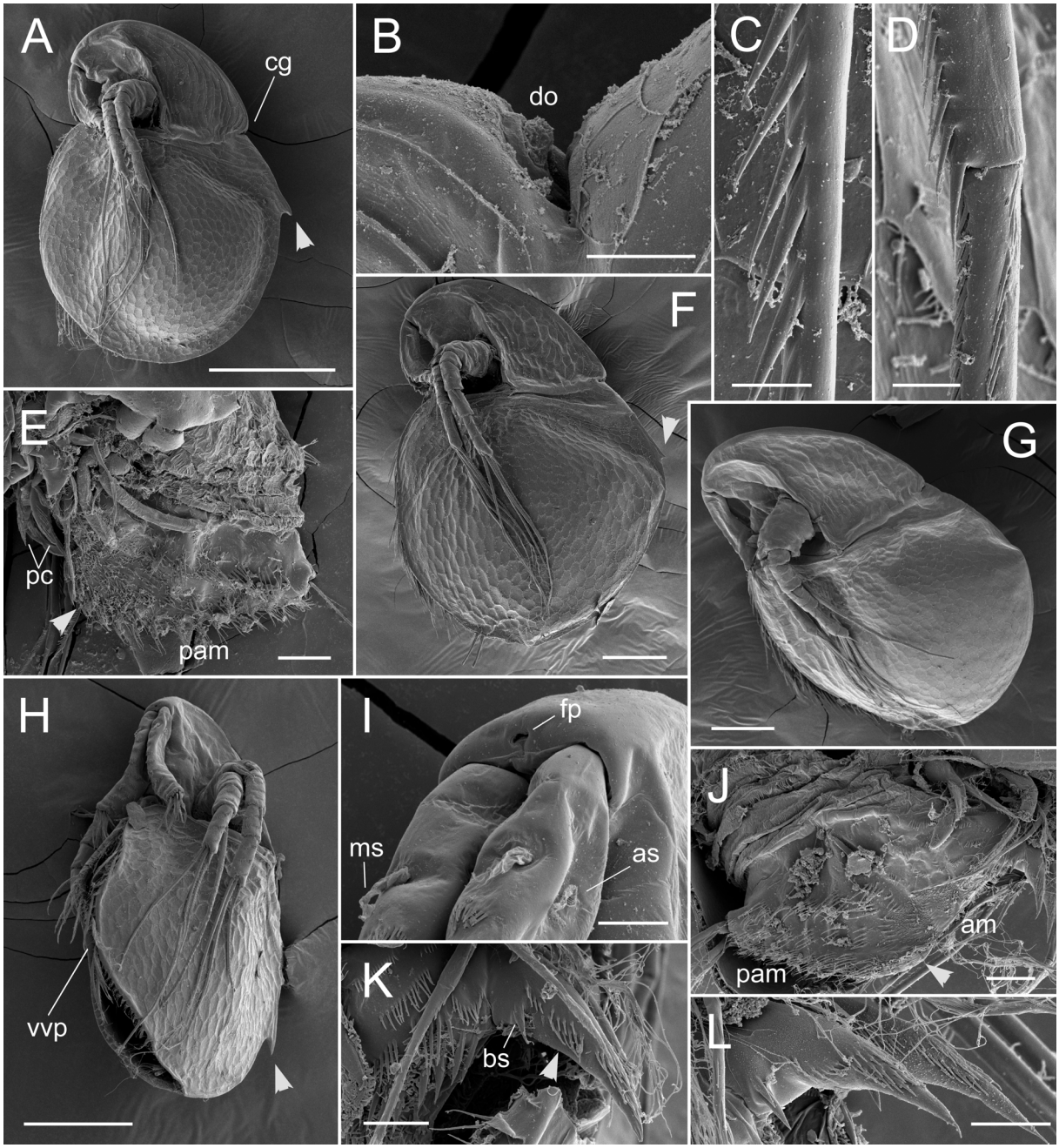

Fig. 2. *Drepanothrix dentata* (Eurén, 1861) from Lake Glubokoe, Moscow Area, Russia (IEE AAK M–7018) (scanning electron micrographs). **A–E**. Adult parthenogenetic female. **A**. General lateral view (white arrow indicates position of dorsal tooth). **B**. Dorsal organ in lateral view. **C**. Swimming seta of endopodite basal segment. **D**. Swimming seta of endopodite second segment. **E**. Postabdomen in lateral view (white arrow indicates position of preanal angle). **F–G**. Ephippial female. **F**. Lateral view (white arrow indicates position of dorsal tooth). **G**. Dorso-lateral view. **H–L**. Male. **H**. General ventro-lateral view (white arrow indicates position of dorsal tooth). **I**. Base of antennae I, ventral view. **J**. Postabdomen in lateral view (white arrow indicates position of preanal angle). **K–L**. Postabdominal claws in outer view (white arrow indicates proximal cluster of spinulae). Abbreviations: am = anal margin of postabdomen; as = basal seta of antenna I; bs = basal spine of postabdominal claw; cg = cervical groove; do = dorsal organ; fp = frontal head pore; ms = male accessory seta; pam = preanal margin; pc = postabdominal claw; vvp = ventral valve projection. Scale bars: A = 200 µm. B, I, K–L = 10 µm. C–D = 5 µm; E, J = 20 µm; F–H = 100 µm.

segments 1 and 2 subequal in length, stout; segment 3 is 1.8–1.9 × as long as endopodal segment 2. All segments of the antennal branches are armed with transverse clusters of setulae. Antenna II seta formula is 0–0–0–3/1–1–3. Swimming seta of the endopodal segment 1 is unisegmented, sclerotized, armed with thick spinulae (Figs 2C, 4D). Swimming seta of the endopodal segment 2 is bisegmented, with distal portion armed with thin spinulae (Figs 2D, 4F). Swimming setae of exopodite and endopodite distal segments are subequal in length. Two posterior setae of each apical segment bear a longitudinal row of spinulae on posterior side (Fig. 4E). The anteriormost seta of each segment has a naked basal segment (Fig. 4G). All apical swimming setae have distal portions with the anterior row of long sparse setulae (gap is ~5 µm) and posterior row of short dense setulae (gap is ~1 µm) (Fig. 4E–G). Antenna II spine formula is 0–1–0–1/0–0–1 (Fig. 4C); spine lengths relative to their segments: exopodal segment 2, 0.5 ×; exopodal segment 4, 0.35 ×; endopodal segment 3, 0.35 × (Fig. 4C).

Mandible. Relatively large, 2.8–3.1 × eye diameter. Mandible molar surfaces are asymmetrical (Fig. 4J–K). Right mandible molar plate is elongated, equally wide anterior and posterior, with a slightly concave

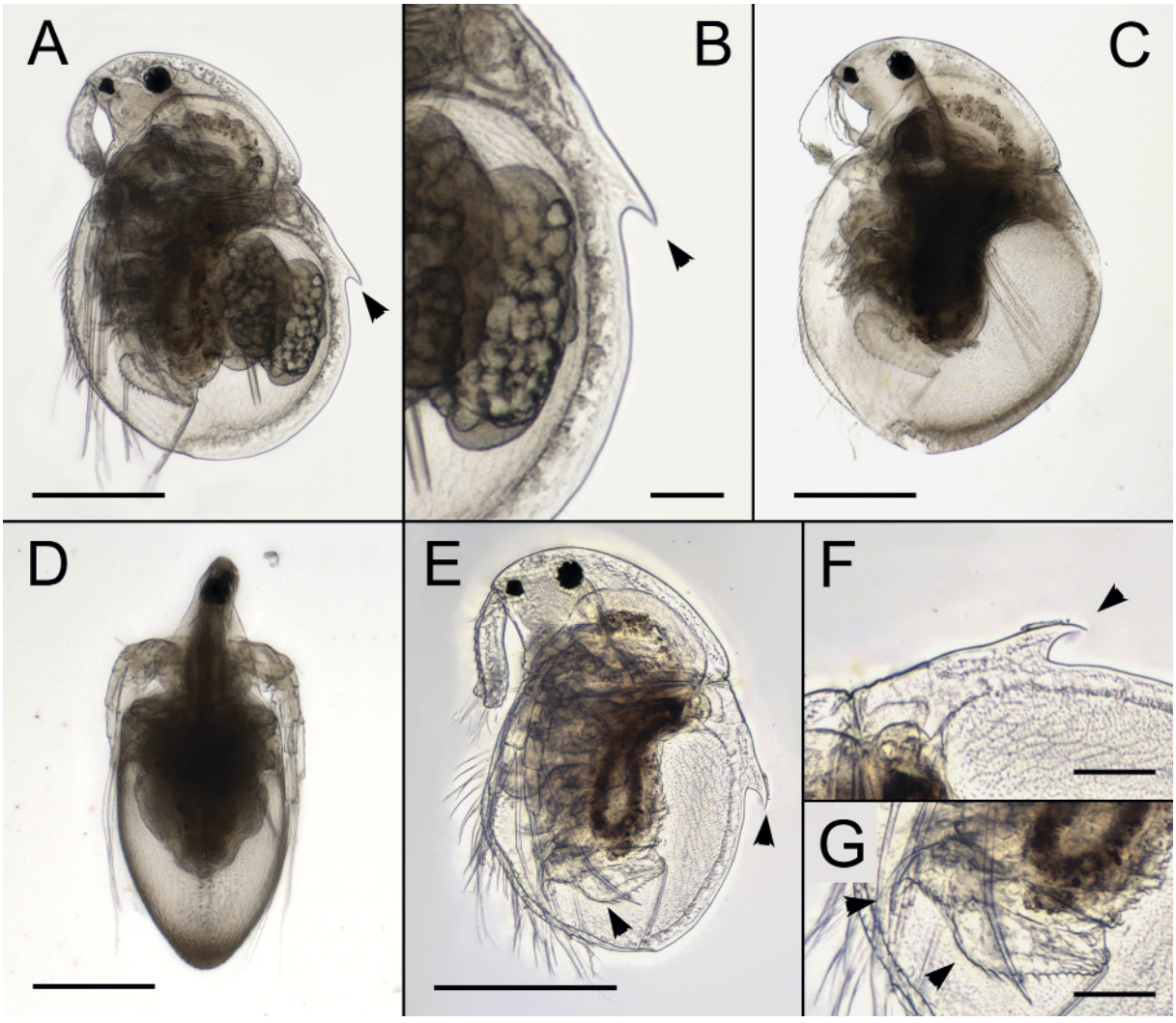

Fig. 3. Optical micrographs of *Drepanothrix dentata* (Eurén, 1861) from Lake Glubokoe, Moscow Area, Russia (IEE AAK M–7018). **A–B**. Parthenogenetic female. **A**. Lateral view. **B**. Dorsal tooth. **C–D**. Ephippial female. **C**. Lateral view. **D**. Dorsal view. **E–G**. Male. **E**. Lateral view. **F**. Dorsal tooth. **G**. Postabdomen. Black arrows indicate diagnostic features of *D. dentata*. Scale bars: A, C–E = 200 µm; B, F–G = 50 µm.

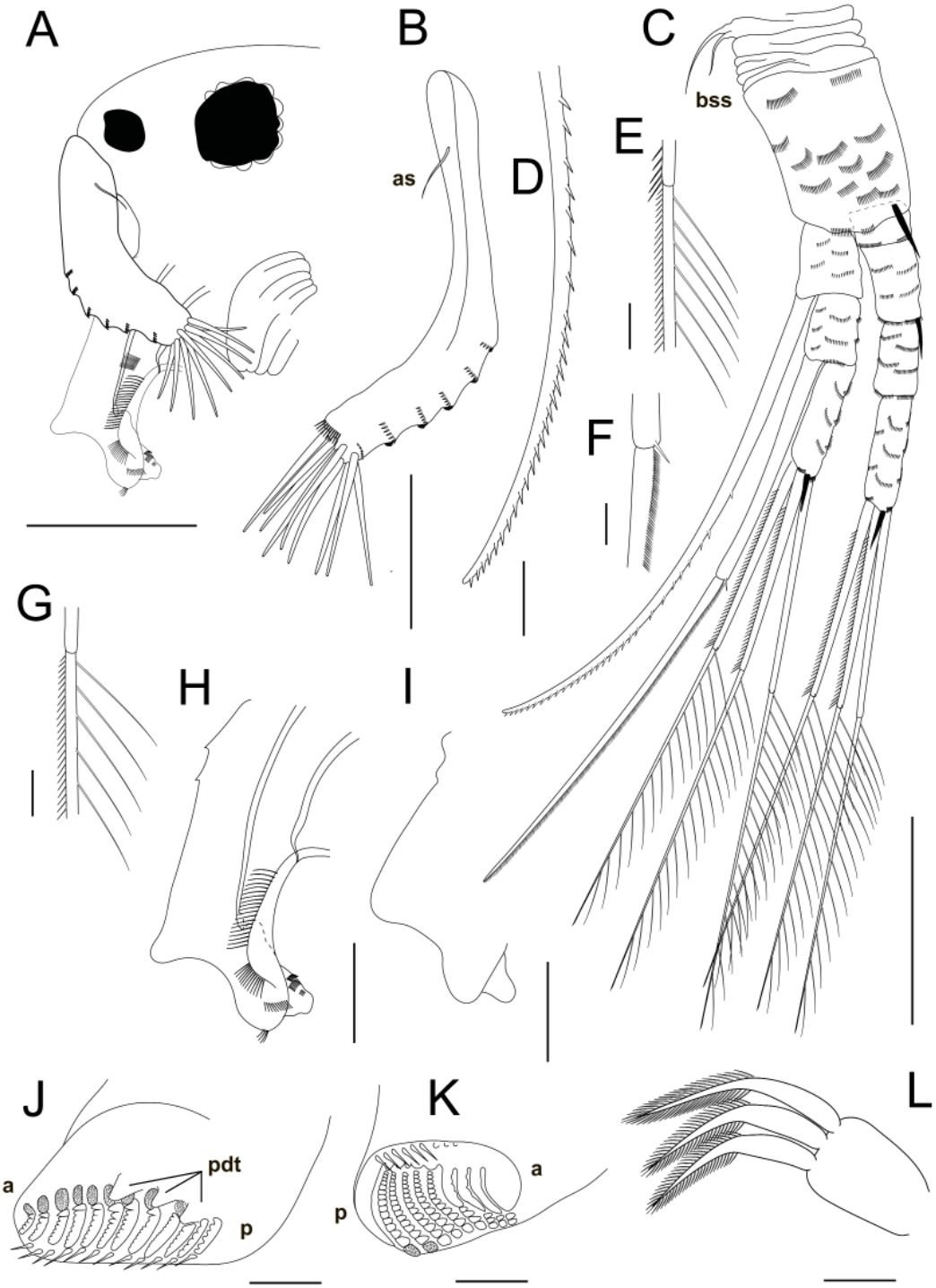

Fig. 4. *Drepanothrix dentata* (Eurén, 1861) from Lake Glubokoe, Moscow Area, Russia (IEE AAK M–7018). **A**. Head, lateral view. **B**. Left antenna I, anterior view. **C**. Right antenna II, lateral view. **D**. Swimming seta of the antenna II endopodal segment 1, enlarged section. **E**. Posterior swimming seta of the antenna II endopodal segment 3, enlarged section. **F**. Swimming seta of the antenna II endopodal segment 2, enlarged section. **G**. Anterior swimming seta of the antenna II endopodal segment 3, enlarged section. **H–I**. Labrum. **J**. Molar plate of the right mandible. **K**. Molar plate of the left mandible. **L**. Maxilla I. Abbreviations: a = anterior; as = antennular seta; bss = basal sensory setae of the antenna II; p = posterior; pdt = posterodorsal teeth of the mandibular plate. Scale bars: A, C = 100 μm; B, H–I = 50 μm; D = 20 μm; E–G, J–L = 10 μm.

ventral margin (Fig. 4J). Plate surface bears 10–12 transverse rows of lamellar outgrowths, and three large conical bumps, located on the dorsoposterior side (Fig. 4J). Left mandible molar plate is short and wide, with posterior edge slightly wider than the anterior (Fig. 4K). Left mandible molar plate is armed with 10–11 transverse rows of outgrowths decreasing in size towards the ventral margin of the molar plate (Fig. 4K).

Maxilla I. Small, spatulate, bearing three setae bilaterally setulated along their entire length (Fig. 4L). Maxilla II is absent.

Five pairs of thoracic appendages differing in size and structure, as follows (Fig. 5).

Thoracic limb I. The largest and comprises an epipodite, an outer distal lobe (ODL), an inner distal lobe (IDL), three inner endites, and a maxillary process (Fig. 5A). The ODL bears two setae (a–b): seta a is very short, located subapically, setulose; seta b is long and thick, located apically; distal portion of seta b is unilaterally armed with short closely spaced setulae (Fig. 5A). The limb I IDL has three setae (1–3). Seta 1 is bisegmented, with the distal portion armed with a row of short spinulae; seta 2 is similar in structure but shorter; seta 3 is the shortest, naked. Limb I inner endites are armed with three anterior setae and 10 posterior setae. Endite 4 bears three posterior setae (4–6) and one anterior seta (1'). Seta 1' is long, unilaterally armed with long setulae. Endite 3 bears three posterior setae (7–9) and one anterior seta (2'). Seta 2' is as long as seta 1', unilaterally armed with short thin spinulae (Fig. 5A–B). Endite 2 bears four posterior setae (10–13) and one anterior seta (3'). Seta 3' is longer than setae 1' and 2', unilaterally armed with short thin spinulae (Fig. 5A, C). Limb I maxillary process with 2 setae.

Thoracic limb II. Comprises a short epipodite, an exopodite, an inner portion, and a gnathobase (Fig. 5D). Exopodite bears three setae (a–c). Seta a is the longest, bilaterally armed with long sparse setulae; seta b is 0.7 × as long as seta a, with distal portion bilaterally armed with short closely spaced setulae; seta c is 0.4 × as long as seta a, armed similarly as seta b. Inner portion has eight anterior scraping setae (1'–8') and two posterior setae (1–2). Scrapers 1' and 2' are the longest, armed with short setulae. Scrapers 3'–5' are subequal in size, 0.7 × as long as scraper 1', the scrapers 3'–5' are armed with thick spines. Scrapers 6'–8' are short, decreasing in length towards posterior; the scraper 6' is armed with thin spinulae, the scrapers 7' and 8' bear dense setulae. Seta 1 is located at the base of scrapers 4' and 5'; seta 1 has a unilateral armature of long setulae. Two short, rounded lobes are located at the posterior limb side, distally to seta 1. Seta 2 is located at the base of scraper 8'; seta 2 is as long as seta 1, densely setulated (Fig. 5D–E). Gnathobase bears six uniform posterior filtering setae and four anterior elements (α–δ): α is a short naked seta, β is a relatively long naked seta with an expanded basal portion, γ is a bottle-shaped sensillum, δ is a short naked seta (Fig. 5D). A row of long setulae is located at the posterior gnathobase side.

Thoracic limb III. Large, comprising an epipodite, an exopodite, an inner portion, and a gnathobase (Fig. 5F–G). Exopodite is elongate, subrectangular, bearing five setae (a–e). Seta a is relatively short, unisegmented, setulated distally. Seta b is 2.2 × as long as seta a, geniculate, with the distal portion armed with short setulae. Seta c is 1.2 × as long as seta a, bilaterally armed with long setulae along its entire length. Seta d is the longest, 2.9–3.0 × as long as seta a, 1.3–1.5 × as long as seta b, 2.5 × as long as seta c, 3.8 × as long as seta e. Seta d is armed with short dense setulae along its entire length. Seta e is slightly shorter than seta a, bilaterally armed with short spinulae (Fig. 5F). Inner endites bear seven anterior setae (1'–7') and nine posterior setae (1–9) (Fig. 5F). Seta 1' is the longest, thin, naked. Seta 1 is 0.8 × as long as seta 1', geniculate, with the distal portion armed with short setulae. Setae 2–4 are similar in size and structure, 0.7 × as long as seta 1', stout, bilaterally armed with long setulae along their entire length. Seta 2' is 0.7 × as long as seta 1', thin. Setae 5–8 are similar in structure, subequal in length to seta 1, naked. Seta 3' is 0.5 × as long as seta 2', setae 4'–7' are similar in length, 0.6 × as long as seta 2' (Fig. 5G). A

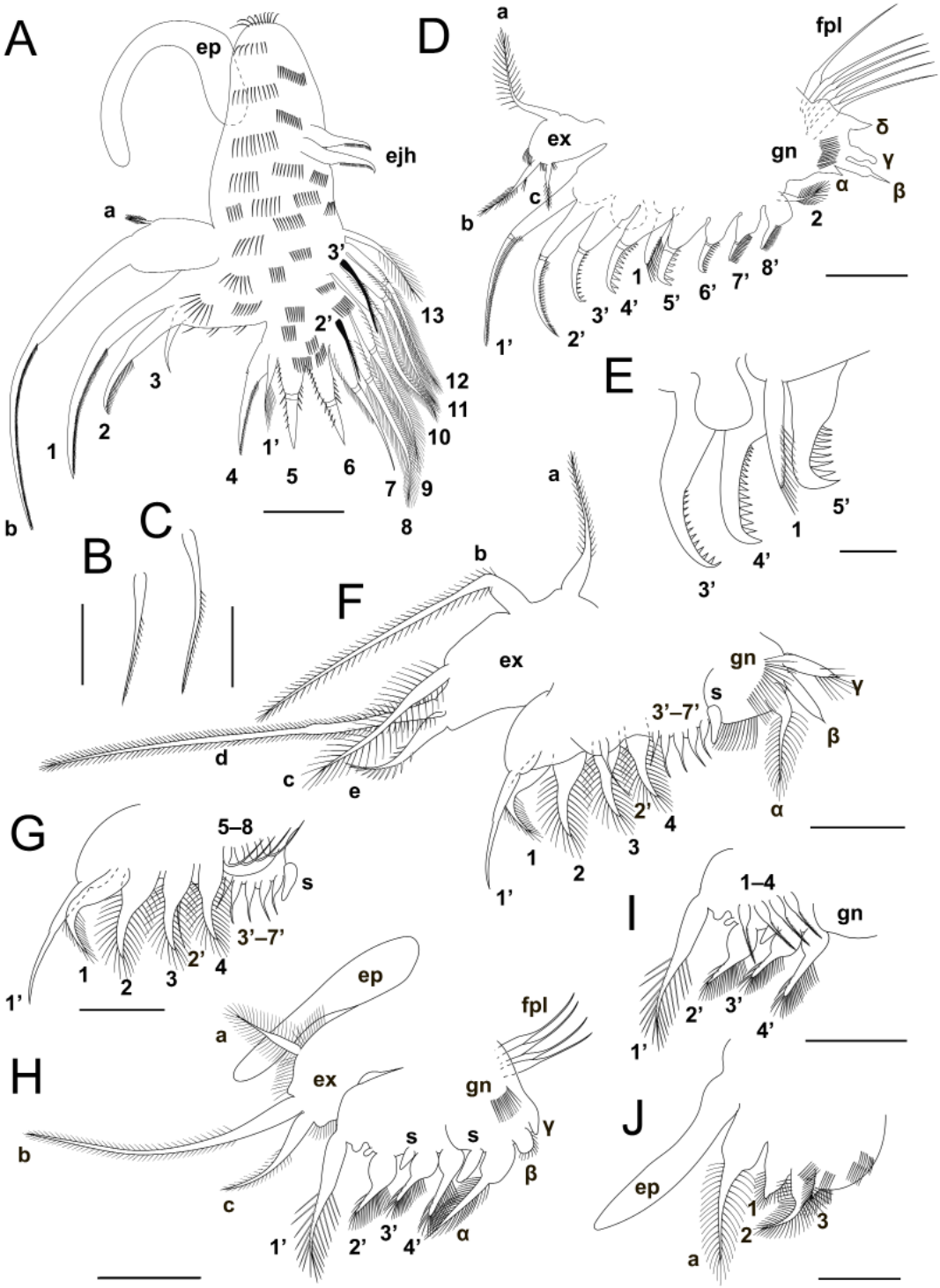

Fig. 5. *Drepanothrix dentata* (Eurén, 1861) from Lake Glubokoe, Moscow Area, Russia (IEE AAK M–7018), thoracic limbs. **A–C**. Thoracic limb I. **A**. General anterior view (limb is flattened). **B**. Seta 2'. **C**. Seta 3'. **D–E**. Thoracic limb II. **D**. General anterior view. **E**. Enlarged portion of the inner endites in posterior view. **F–G**. Thoracic limb III. **F**. General anterior view. **G**. Inner endites in posterior view. **H–I**. Thoracic limb IV. **H**. General anterior view. **I**. Inner endites, posterior row of setae. **J**. Thoracic limb V. Abbreviations: ejh = ejector hooks; ep = epipodite; ex = exopodite; fpl = filtering plate of the gnathobase; gn = gnathobase; s = sensillum. For seta labeling, see Material and methods. Scale bars: A, D, F–J = 20 μm; B–C, E = 10 μm.

large oval sensillum is located proximally to setae 3'–7'. A small, rounded lobe is located anteriorly between the bases of setae 5' and 6' (Fig. 5F). The gnathobase bears three large anterior elements: a long geniculate seta bilaterally armed with long setulae (α), and two cylindrical sensilli with acute apex (β, γ); the sensillum γ bears a group of setulae at the tip (Fig. 5G).

Thoracic limb IV. Large, comprising an epipodite, an exopodite, an inner portion, and a gnathobase (Fig. 5H). Exopodite is rounded, bearing three setae (a–c). Seta a is short, bilaterally armed with long setulae along its entire length; seta b is 4.0 × as long as seta a, with a distal armature of short setulae; seta c is 2.4 × as long as seta a, similar in structure to seta b. Inner portion has four anterior setae (1'–4') and four posterior setae (1–4). Seta 1' is the longest, with a distal armature of long spinulae. Setae 2'–4' are similar in structure, scraper-like, with an expanded base and a blunt tip, bearing an asymmetrical armature of long closely-spaced flattened spinulae. Setae 2' and 3' are subequal in length, 0.5 × as long as seta 1; seta 4' is 0.6 × as long as seta 1 (Fig. 5H–I). A small, rounded lobe is located distally to the base of seta 2'. A conical sensillum is located between the bases of setae 2' and 3'; a large oval sensillum proximally to the base of seta 4'. Setae 1–4 are similar in structure, short, distally armed with very short setulae (Fig. 5I). The gnathobase has a filtering comb of four uniform posterior setae, and three anterior elements: a long seta with an expanded base and distal armature of long setulae (α), a short rounded setulated lobe (β), and a short naked seta (γ) (Fig. 5H).

Thoracic limb V. Strongly reduced, comprising an epipodite, an exopodite, and an inner portion with three setae (Fig. 5J). Exopodite bears a single seta (a) with an expanded base; seta a is distally armed with long sparse setulae. Inner portion has three setae densely armed with long setulae: setae 1 and 3 are very short and wide, seta 2 is 0.6 × as long as seta a (Fig. 5J).

Ephippial female

Body. Length is 0.55–0.70 mm (Figs 1E, 2F–G). Morphology is similar to that of the parthenogenetic female, except as noted below (Figs 1E, 2F–G, 3C–D). Body is flattened laterally (height : length = 0.7–0.8; width : length = 0.3–0.4). Dorsal keel of carapace is reduced (Figs 1E, 2F–G, 3C). Dorsal carapace margin is slightly angulate in lateral view (Figs 1E, 2F–G). Dorsal tooth is strongly reduced or absent (Figs 1F–G, 2F–G, 3C). Ephippium lacks a specific sculpture and clear ventral border (Figs 2F–G, 3C). Ephippium contains two resting eggs.

Male

Body. Length is 0.45–0.70 mm (Figs 1H, 2H). Body is ovoid in lateral view, flattened laterally (height : length = 0.6–0.7; width : length = 0.3–0.35). General morphology is largely similar to that of the juvenile parthenogenetic female (Figs 1H, 2H, 3E). Dorsal keel is well developed in both head and valves (Figs 1H, 3E). Dorsal tooth is large, slightly incurved posteriorly (Figs 1H, 2H, 3E–F). Posterodorsal carapace angle is well pronounced (Figs 1H, 3E). Ventral valve margin forms a wide rounded projection at the level of thoracic limb I (Fig. 3E). Carapace ornamentation is similar to that of parthenogenetic female (Fig. 2H).

Postabdomen. Relatively small, 0.3 × as long as body, flattened laterally. Postabdomen is generally similar in shape to that of the female (Figs 1I, 2J, 3E). Postabdomen is subquadrangular in lateral view; preanal postabdomen portion has approximately parallel dorsal and ventral margins (Figs 1I, 2J, 3G). Preanal angle is almost right, shifted towards the anal opening (Figs 1I, 3G). Preanal margin is armed with 9–10 transverse rows of setulae anterior to the preanal angle and with only 2–3 rows posterior to the preanal angle (Figs 1I, 2J). Lateral surface of the preanal postabdomen portion bears transverse clusters of setulae, forming three longitudinal rows: dorsal setulae, long anteriorly to the preanal angle and short posteriorly to the preanal angle; medial setulae, relatively short, not reaching postabdomen base; marginal setulae, long anteriorly to the preanal angle and short posteriorly to the preanal angle

(Figs 1I, 2J). The anal portion of the postabdomen is longer than in the female, measuring 0.3–0.4 × as long as preanal portion. Anal margin forms an angle with preanal margin posterior portion. A distinct depression is present between preanal and anal margins (Figs 1I, 2J, 3G). Anal portion bears 2–3 clusters of spines and several longitudinal groups of short setulae (Fig. 1I). Postabdominal claw is relatively short and wide, 0.3 × as long as the postabdomen, 2.7–3.2 × as long as wide, slightly incurved (Figs 1J–K, 2K–L). Lateral claw surface bears two clusters of short spinulae which do not form pectens (Figs 1J–K, 2K–L). Basal spine of the claw is relatively short, 0.4–0.5 × as wide as postabdomen. A shorter spine is usually located at the base of the basal spine, resulting in a double basal spine (Figs 1J–K, 2K–L). Vas deferens runs along the ventral postabdomen margin, opening subterminally at a low projection (Fig. 1I). Gonopores are in sublateral position (Fig. 1I).

Antenna I. Resembles that of parthenogenetic female but bears an additional seta in its proximal portion. Male accessory seta is located on the anterior edge of the antenna I; the seta is short and thick (Figs 1J, 2I).

Antenna II. Similar to that of parthenogenetic female but has two additional sensory setae at the distal end of the basipodite; the setae exceed the length of the distal burrowing spine (Figs 1J, 2H).

Thoracic limbs. Mostly similar to that of the parthenogenetic female, with the exception of limb I.

Limb I. Modified compared to that of the female (Fig. 1L–M). The anterior surface of limb I forms a small subdistal lobe (SDL) armed with three transverse rows of spinulae. The SDL also bears two setae (X, Y) approximately equal in length; seta X is naked, while seta Y has a distal armature of short setulae (Fig. 1L–M). The IDL bears a large hook extending beyond the tip of the SDL; inner side of the hook apex is armed with three cuticular rows. The IDL has four setae: seta 1 is the longest, with distal portion armed with short setulae; seta 2 is 0.65 × as long as seta 1, armed with short setulae; seta 3 is 0.7 × as long as seta 1, naked; male accessory seta (Z) is short (SZ/S1 = 0.30–0.35), naked (Fig. 1L). The ODL, inner endites and maxillary process are similar in structure to those of the parthenogenetic female, except for the absence of the anterior seta 1' (Fig. 1L).

Remarks

Drepanothrix dentata widely occurs in Europe (Błedzki & Rybak 2016) and European Russia eastward to the Nenets Autonomous Region, Russia (Smirnov 1976). However, the species is very rare (Błedzki & Rybak 2016); thus, its eastern distribution border remains unclear. However, representatives of *Drepanothrix* are likely absent in Cis- and Transcaucasia (Behning 1947) and Kazakhstan (Ibrasheva & Smirnova 1983). Multiple records of *D.* cf. *dentata* from North America (Herrick 1884; Birge 1892, 1918; Herrick & Turner 1895; Bigelow 1922; Brooks 1959; Smirnov 1976; Smith 2001; Elías-Gutiérrez *et al.* 2018; GBIF Secretariat 2023) likely represent a particular lineage (see "Genetic variability" section below). The species inhabits water bodies of different types and occurs mostly in bottom sediments of the vegetated zone (Błedzki & Rybak 2016), being able to burrow into the upper layer of sediments (Fryer 1974; Kotov 2006).

Drepanothrix asiatica sp. nov.

urn:lsid:zoobank.org:act:5C94EEB5-2164-4162-B604-DC7AC93BE9CC

Figs 6–13

Drepanothrix dentata – Smirnov 1976: 164, fig. 149b; 1992: 119–121, figs 504–509. — Yermolayeva & Fetter 2020: fig. 2a–c.

Drepanothrix cf. *dentata* – Dadykin *et al.* 2025: fig. s1.

Diagnosis

In the parthenogenetic female and male, dorsal valve margin has a strongly reduced dorsal tooth, or the latter is completely absent. Male postabdomen is strongly modified as compared to that of the female. Preanal angle of the postabdomen is oblique, shifted towards the postabdomen base. Male postabdominal claw is long and slender. Male postabdominal claw bears a basal pecten and a distal cluster of spinulae.

Etymology

The species name '*asiatica*' refers to its distribution in Asia.

Type material

Holotype

RUSSIA • ♂; Kamchatskii Krai, Kronotsky Nature Reserve, a small drying thermokarst lake; 54°13.921′ N, 160°9.696′ E; 21 Aug. 2014; E.I. Bekker and F.V. Kazansky leg.; MSU, MGU MI–287.

Allotype

RUSSIA • 1 ♀; same data as for holotype; MSU, MGU MI–288.

Paratypes

RUSSIA • 17 parthenogenetic ♀♀; same data as for holotype; MSU, MGU MI–289 • 5 parthenogenetic ♀♀, 6 ♂♂; same data as for holotype; ZIN, ZIN 55222 • 3 parthenogenetic ♀♀, 2 ephippial ♀♀, 5 ♂♂; same data as for holotype; IEE, IEE AAK 2026–012 • 6 parthenogenetic ♀♀; Sakhalin Area, Kuril Archipelago, a small sphagnal bog in Simushir Island; 47°7.088′ N, 152°16.452′ E; 22 Jul. 2019; M.O. Ivanova leg.; ZIN, ZIN 55223 • 7 parthenogenetic ♀♀; same data as for preceding; IEE, IEE AAK 2026–011.

Other material examined

RUSSIA • 6 parthenogenetic ♀♀; Khabarovskii Krai, a small lake at eastern shore of the Nikolay Bay; 53°54.000′ N, 138°41.770′ E; 27 Aug. 2021; O. Shpak leg.; IEE, IEE AAK M–7069 • 4 parthenogenetic ♀♀; same data as for preceding; ZIN, ZIN 55224 • 3 parthenogenetic ♀♀; Sakhalin Area, Sakhalin Island, a sphagnal lake near Pokrovka Village; 47°19.234′ N, 142°42.432′ E; 15 Sep. 2008; A.A. Kotov and N.M. Korovchinsky leg.; IEE, IEE AAK M–0864 • 3 parthenogenetic ♀♀; Sakhalin Area, Kuril Archipelago, a small sphagnal bog in Simushir Island; 47°6.040′ N, 152°14.262′ E; 22 Jul. 2019; M.O. Ivanova leg.; IEE, IEE AAK M–6526 • 11 parthenogenetic ♀♀, 1 ♂; same data as for preceding; 47°7.088′ N, 152°16.452′ E; same data as for preceding; IEE, IEE AAK M–6527 • 5 parthenogenetic ♀♀; Kamchatskii Krai, Kronotsky Nature Reserve, a small thermokarst lake; 54°14.162′ N, 160°9.756′ E; 21 Aug. 2014; E.I. Bekker and F.V. Kazansky leg.; IEE, IEE AAK M–3029 • 1 parthenogenetic ♀; same data as for preceding; IEE AAK M–3028 • 3 parthenogenetic ♀♀; Kamchatskii Krai, Karaginsky Island, a small slightly brackish lake; 58°33.621′ N, 163°29.034′ E; 16 Jul. 2022; I.A. Dadykin leg.; IEE, IEE AAK M–7655 • 2 parthenogenetic ♀♀; Kamchatskii Krai, Karaginsky Island, a small lake with muddy sediment; 58°58.135′ N, 163°53.052′ E; 5 Aug. 2022; I.A. Dadykin leg.; IEE, IEE AAK M–7720 • 3 parthenogenetic ♀♀; Kamchatskii Krai, Bering Island, a small tundra lake near Nikolskoe Village; 55°13.291′ N, 166°0.654′ E; 28 Sep. 2020; O. Krylovich, E. Kuzmicheva and O. Smyshlyaeva leg.; IEE, IEE AAK M–6493 • 1 parthenogenetic ♀; Chukotskii Autonomous Region, a small pool in the vicinity of Anadyr River; 65° N, 171° E; 7 Aug. 1972; N.N. Smirnov leg.; MSU, MGU MIs 1178.

Description

Parthenogenetic female

Body. Length 0.35–0.8 mm. Body is ovoid in lateral view (length : height = 0.66–0.75), flattened laterally (width : length = 0.35–0.42) (Figs 6A–B, 7A–C, 8A–B, F–H). Dorsal keel is well pronounced in both head anterior portion and valves, but is absent in posterior head portion (Fig. 7B). A deep cervical groove is located on each lateral side, preceded by a transverse cuticular ridge (Figs 6B, 7B). The cervical grooves do not intercept dorsally. Dorsal tooth is usually absent; very rarely a minute tooth is present (Figs 6A, C–G, 7A, 8A–B, F–I). Posterodorsal body angle is widely rounded; ventral body margin is evenly convex (Figs 6A, 7A). Carapace is ornamented with irregular polygons becoming more elongate towards the ventral and posterior valve margins (Figs 6A, 7A, D). Ventral valve margin bears a row of 35–40 flattened cuticular flanges subequal in size, which do not reach the posterodorsal valve angle (Fig. 7A, E). A long feather-like seta is attached posteriorly to each flange at the inner side of the valve margin (Fig. 7E). A cluster of setulae runs along the inner side of the valve margin, along the flange (Fig. 7E).

Head. Large (HL/BL = 0.49–0.50), strongly flattened laterally (length : width 1.3–1.5). Head shape, compound eye and ocellus conform to the generic diagnosis (Figs 6A–B, H–I, 7A–C). Dorsal organ is as typical for the genus (Figs 6H–I, 7B, H–I). Lateral head pores are absent. Frontal pore is small, horseshoe-shaped, located near the anterodorsal head angle (Fig. 7J). Thorax, gut and abdomen conform to the generic diagnosis.

Postabdomen. Shape and armature conform to the generic diagnosis (postabdomen is 0.2 × as long as the body, 1.3–1.4 × as long as high; preanal margin is 3.5–4 × as long as the anal margin) (Figs 6J, 7F). Postabdominal claw is short and stout, 0.3–0.35 × as long as the postabdomen, 3.6–4.0 × as long as high, slightly incurved. Basal spine of the claw is rather short, 1.0–1.1 × the claw width (Figs 6J–K, 7G). Both the lateral and the medial claw sides bear two clusters of spinulae which do not form distinct pectens (Figs 6K, 7G). Postabdominal setae are as typical for the genus.

Labrum. Large and wide, approximately triangular in lateral view (Figs 9A, 10A). Labrum armature and shape are as typical for the genus.

Antenna I. Conforms to the generic diagnosis (Figs 7A, C, 9A–C, 10B–C). Basal seta of the antenna I is 0.15–0.20 × length of the antenna I. Antenna I apex bears nine terminal aesthetascs of subequal size, 0.31–0.35 × as long as antenna I.

Antenna II. 0.95–1.1 × as long as the body (Figs 6A, 7A). Morphology of antenna II conforms to the generic diagnosis (Figs 9D–I, 10D–H); endopodite is 0.78–0.85 × as long as the exopodite (Figs 9D, 10D). Swimming seta of the endopodal segment 1 is 2.1–2.2 × length of endopodite segments; swimming seta of the endopodal segment 2 is 2.1–2.25 × length of the endopodite segments. Setal armature conforms to the generic diagnosis (Figs 9F–I, 10E–H). Spine lengths relative to their segments: exopodal segment 2, 0.6–0.65 ×; exopodal segment 4, 0.4–0.5 ×; endopodal segment 3, 0.3–0.4 × (Figs 9D, 10D).

Mandible. Large, 2.8–3.1 × eye diameter (Fig. 10J). Mandible armature is as typical for the genus (Fig. 9K–M).

Maxilla I. Small, spatulate, armed with three thick feather-like setae subequal in size (Fig. 9N). Maxilla II is absent.

Thoracic appendages. I–V conform to the generic diagnosis (Figs 10I–J, 11).

Thoracic limb I. As typical for the genus (Figs 10I–J, 11A). The outer distal lobe (ODL) is cylindrical, directed posteriorly, bears two setae (a, b). Seta a is attached subterminally, thin, bisegmented, bilaterally armed with short setulae. Seta b is attached terminally, long, thick, with apical segment armed with a row

of spinulae (Fig. 11A–B). The inner distal lobe (IDL) bears three bisegmented setae (1–3). Seta 1 is the longest, seta 2 is 0.7–0.8 × the length of seta 1; both setae 1 and 2 are armed with a row of setulae. Seta 3 is naked and 0.40–0.45 × the length of seta 1 (Figs 10I–J, 11A–B). Seta 4 slightly exceeds setae 5 and 6 in length; the proximal portion of seta 4 is almost naked, with few apical spines; the distal portion is unilaterally setulated. Setae 5 and 6 are similar in length and structure; both are thick, bilaterally armed with short spinulae not reaching the setal tip (Fig. 11C). Seta 7 is slightly shorter than seta 8; both the proximal and distal portions of seta 7 bear a row of spinulae extending only halfway to the tip (Fig. 11C). Setae 8 and 9 are similar in structure, with proximal portion armed with a row of spinulae, and distal

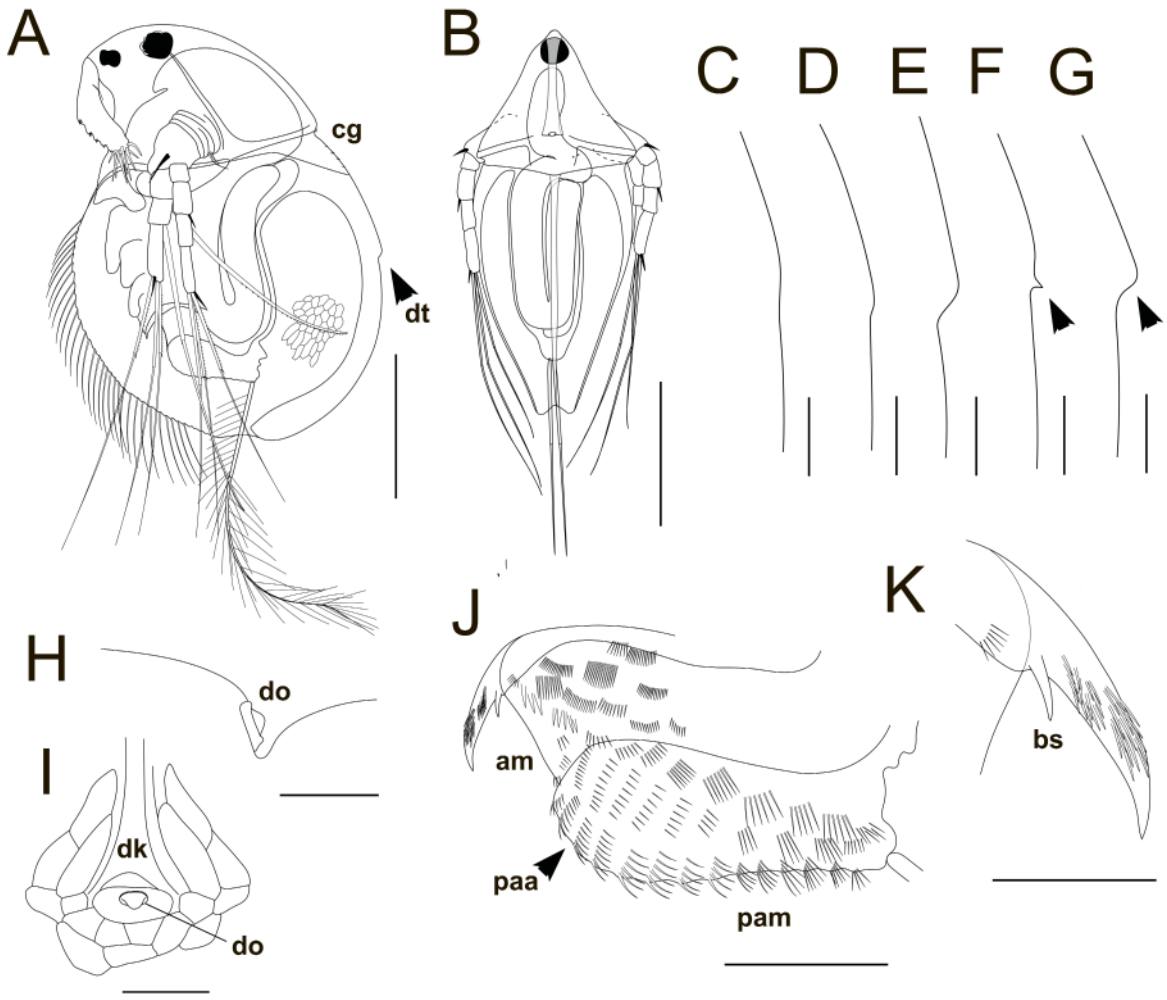

Fig. 6. *Drepanothrix asiatica* sp. nov., morphology of parthenogenetic female. **A–B, H–K**. Parthenogenetic female from the Kronotsky National Reserve, Kamchatskii Krai, Russia (MGU MI–289, type locality). **C–G**. Variation of dorsal tooth morphology in different populations of *D. asiatica*. **A**. General lateral view. **B**. Dorsal view. **C**. Sakhalin Island, Sakhalin Area, Russia (IEE AAK M-6527). **D**. Bering Island, Kamchatskii Krai, Russia (IEE AAK M-6493). **E–F**. Kronotsky National Reserve near type locality, Kamchatkskii Krai, Russia (IEE AAK M-3029), arrow shows a reduced dorsal tooth. **G**. Khabarovskii Krai, Russia (IEE AAK M-7069), arrow shows a reduced dorsal tooth. **H**. Dorsal organ in lateral view. **I**. Dorsal organ in dorsal view. **J**. Postabdomen in lateral view. **K**. Postabdominal claw in lateral view. Abbreviations: am = anal margin of postabdomen; bs = basal spine of postabdominal claw; cg = cervical groove; dk = dorsal keel; do = dorsal organ; dt = dorsal tooth; paa = preanal angle of postabdomen; pam = preanal margin of postabdomen. Scale bars: A–B = 200 μm; C–I, K = 20 μm; J = 50 μm.

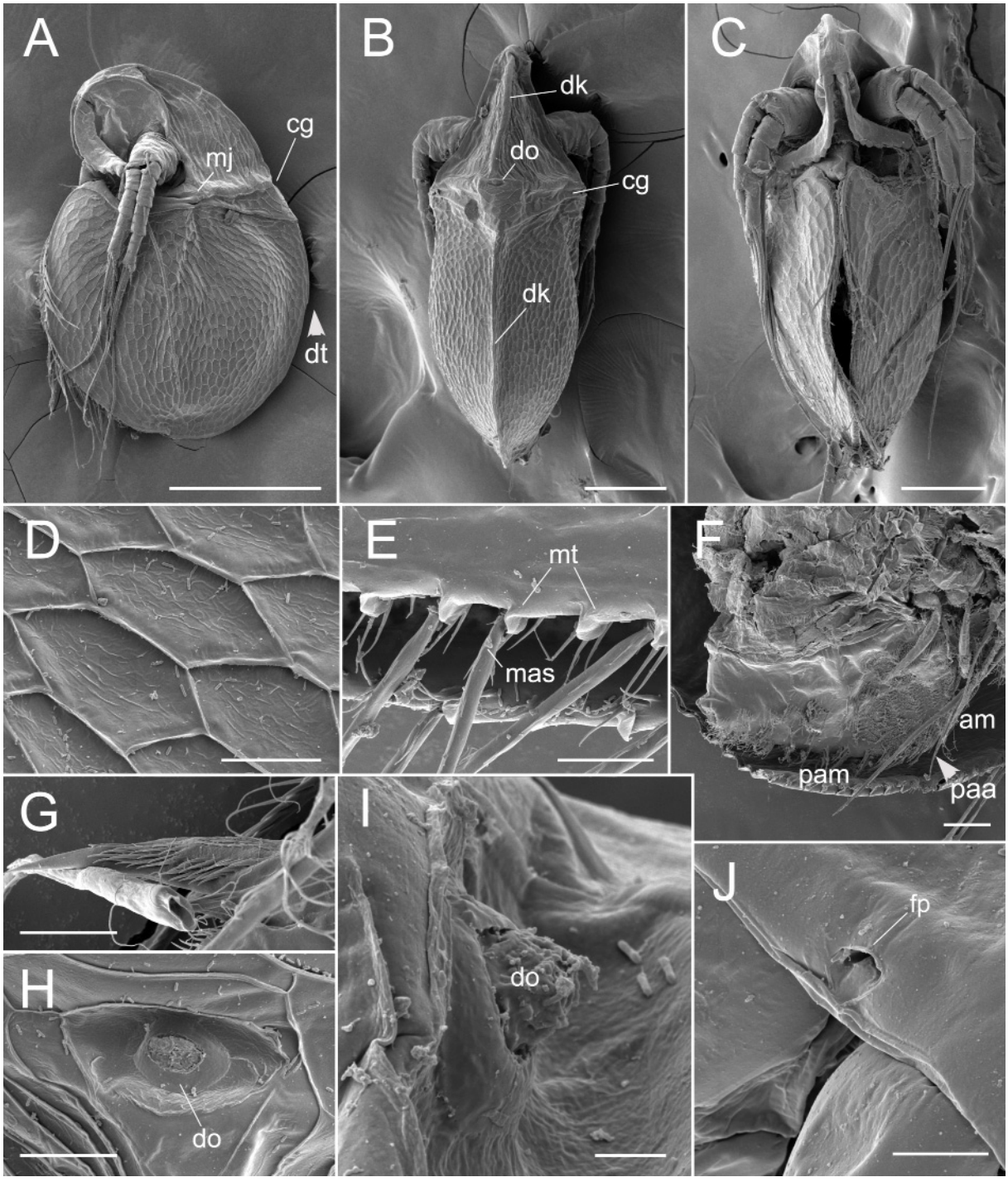

Fig. 7. Scanning electron micrographs of *Drepanothrix asiatica* sp. nov., parthenogenetic female from the Kronotsky National Reserve, Kamchatskii Krai, Russia (MGU MI–289, type locality). **A**. Lateral view. **B**. Dorsal view. **C**. Ventral view. **D**. Valve sculpture. **E**. Armature of ventral valve margin. **F**. Postabdomen in lateral view (white arrow indicates position of preanal angle). **G**. Postabdominal claw, outer view. **H**. Dorsal organ in dorsal view. **I**. Dorsal organ in lateral view. **J**. frontal head pore. Abbreviations: am = anal margin of postabdomen; cg = cervical groove; dk = dorsal keel; do = dorsal organ; dt = dorsal tooth; fp = frontal head pore; mas = marginal valve setae; mj = mandibular joint; mt = marginal valve teeth; paa = preanal angle of postabdomen; pam = preanal margin of postabdomen. Scale bars: A = 200 µm; B–C = 100 µm; D–E, G–H = 10 µm; F = 20 µm; I = 2 µm; J = 5 µm.

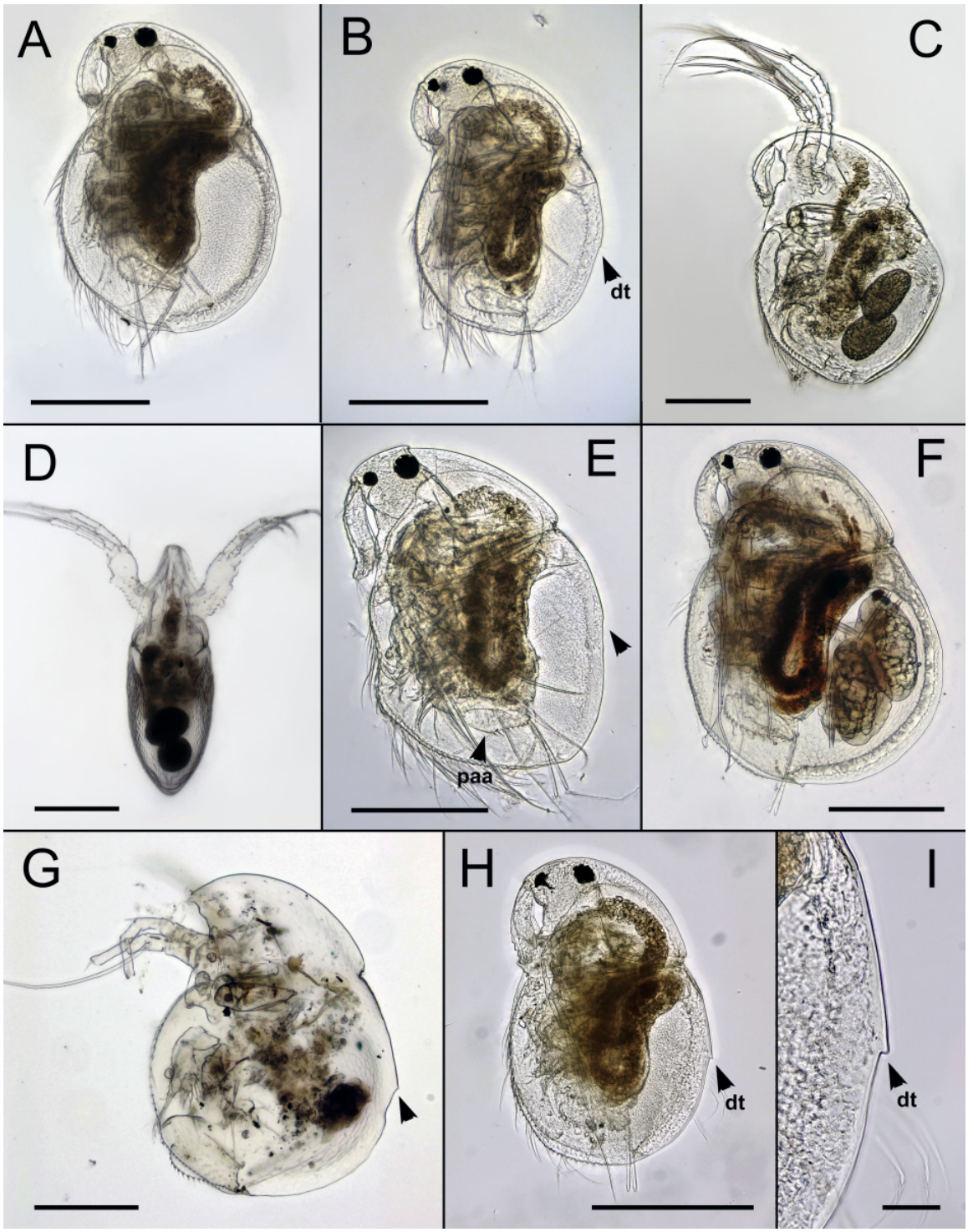

Fig. 8. Optical micrographs of *Drepanothrix asiatica* sp. nov. **A–E**. Type locality in the Kronotsky National Reserve, Kamchatskii Krai, Russia. **A**. Adult parthenogenetic female (allotype MGU MI–288). **B**. Juvenile parthenogenetic female (paratype MGU MI–289). **C–D**. Ephippial female. **E**. Male (holotype MGU MI-287). **F**. Adult parthenogenetic female, Simushir Island, Sakhalin Area, Russia (paratype ZIN 55223). **G**. Adult parthenogenetic female, Sakhalin Island, Sakhalin Area, Russia (IEE AAK M–0864). **H–I**. Juvenile parthenogenetic female, Khabarovskii Krai, Russia (ZIN 55224). Abbreviations: dt = dorsal tooth; paa = preanal angle of postabdomen. Black arrows indicate diagnostic features of *D. asiatica*. Scale bars: A–H = 200 μm; I = 50 μm.

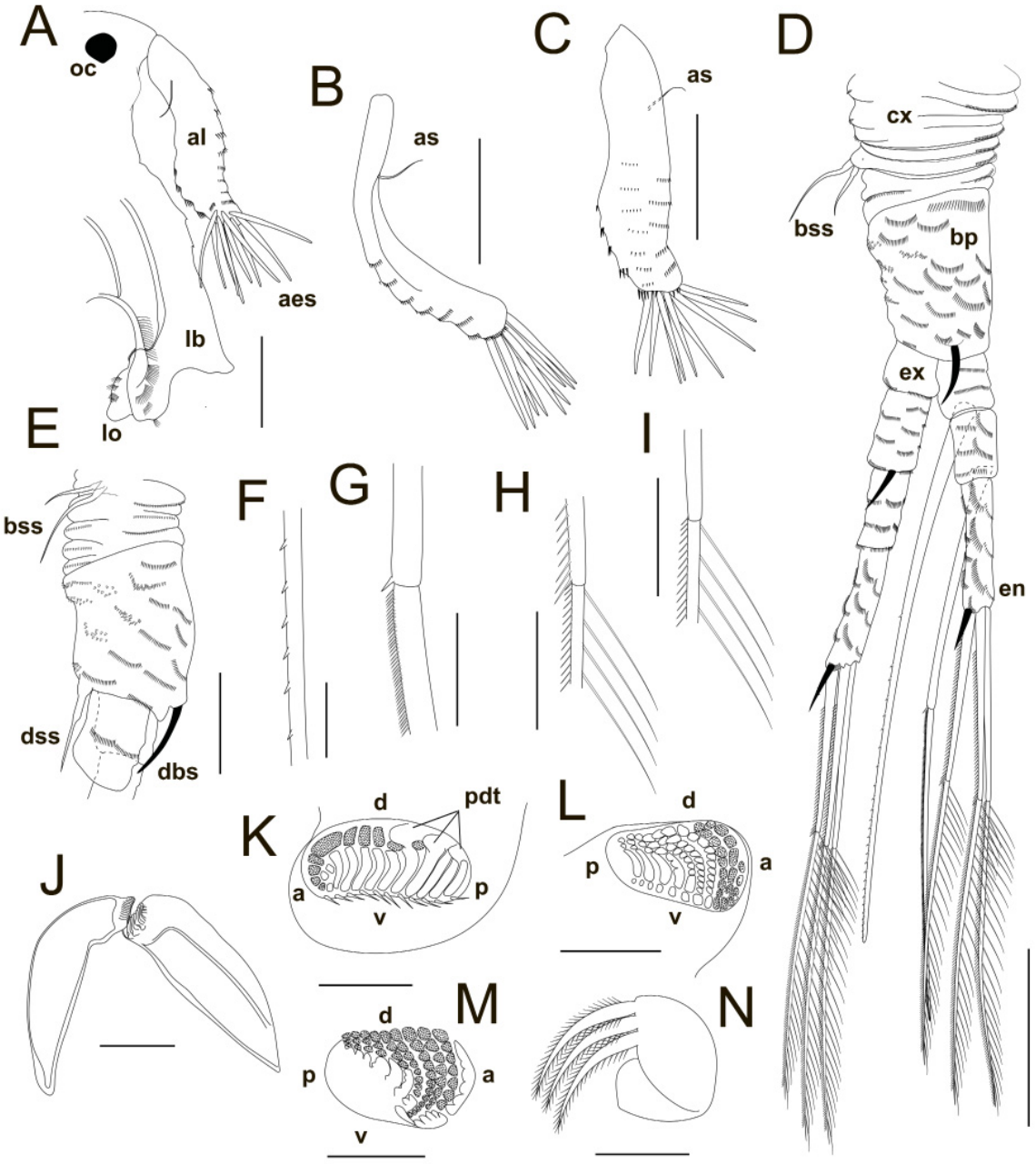

Fig. 9. *Drepanothrix asiatica* sp. nov., parthenogenetic female from the Kronotsky National Reserve, Kamchatskii Krai, Russia (MGU MI–289, type locality). **A**. Ventral head margin in lateral view. **B**. Left antenna I in ventral view. **C**. Left antenna I in proximal view. **D**. Right antenna II in outer view. **E**. Right antenna II base in posterior view. **F**. Armature of basal endopodite segment swimming seta. **G**. Armature of the second endopodite segment swimming seta. **H**. Armature of the exopodite segment posterior seta. **I**. Armature of the apical exopodite segment anterior seta. **J**. Mandibles in frontal view. **K**. Right mandible molar surface. **L–M**. Left mandible molar surface. **N**. Maxilla I. Abbreviations: a = anterior side of mandible molar plate; aI = antenna I; aes = aesthetascs; as = antennular seta; bp = basipodite of antenna II; bss = basal sensory setae of antenna II; cx = coxal part of antenna II; d = dorsal side of mandible molar plate; dbs = distal burrowing spine of antenna II; dss = distal sensory seta of antenna II; en = endopodite of antenna II; ex = exopodite of antenna II; lb = labrum; lo = labral outgrowth; oc = ocellus; p = posterior side of mandible molar plate; pdt = posterodorsal teeth; v = ventral side of mandible molar plate. Scale bars: A–C, E, J = 50 µm; D = 100 µm; F–I, K–N = 20 µm.

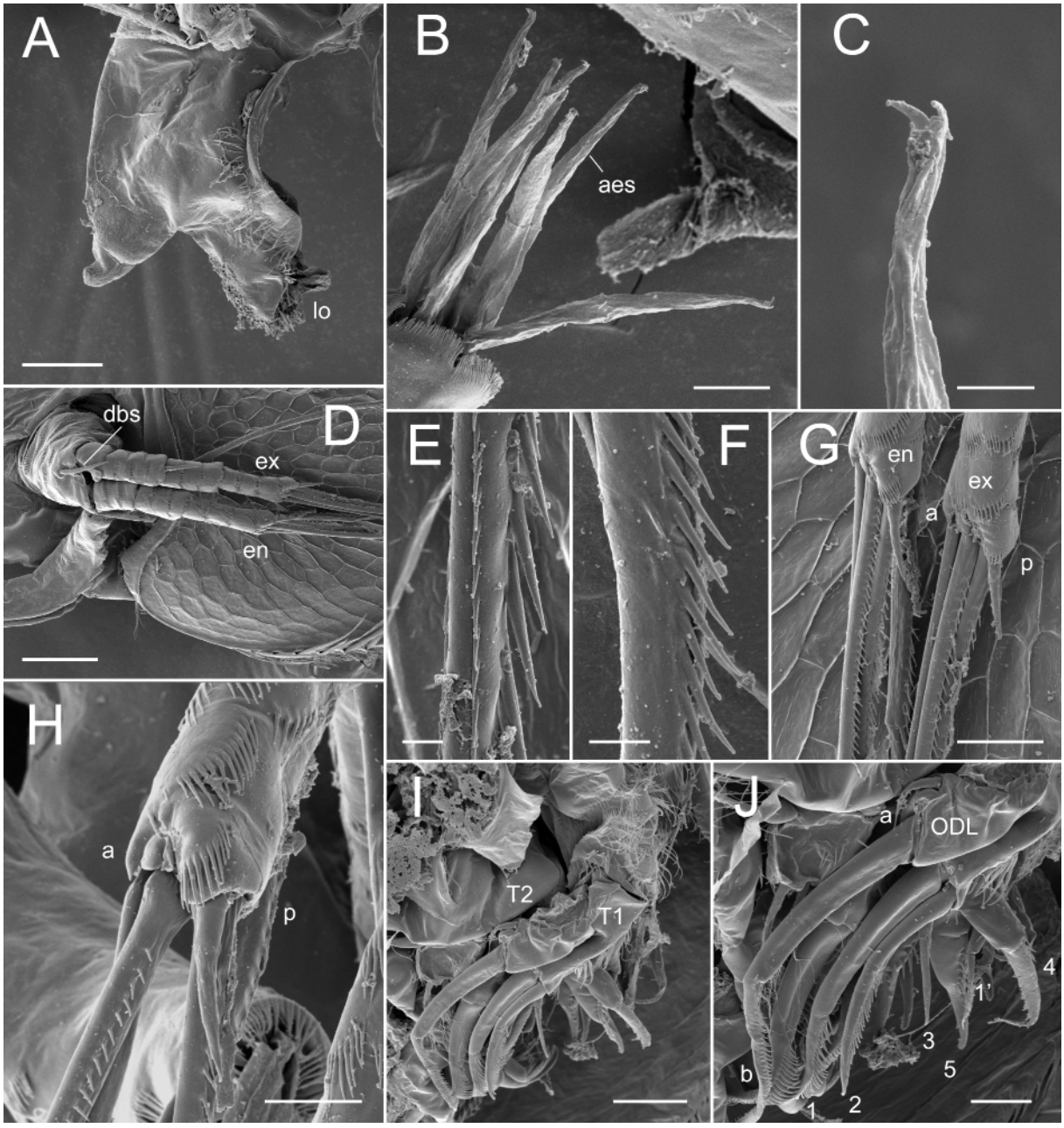

Fig. 10. Scanning electron micrographs of *Drepanothrix asiatica* sp. nov., parthenogenetic female from the Kronotsky National Reserve, Kamchatskii Krai, Russia (type locality, IEE AAK M–3027). **A**. Labrum in lateral view. **B**. Tip of antenna I in outer view. **C**. Tip of the aesthetasc. **D**. Antenna II in lateral view. **E**. Armature of the basal endopod segment swimming seta. **F**. Armature of the second endopod segment swimming seta. **G**. Tips of the antennal branches in lateral view. **H**. Tip of the antennal endopodite in postero-lateral view. **I**. Thoracic limb I in outerview. **J**. Distal portion of the limb I in outer view. Abbreviations: a = anterior side of the antennal branch; aes = aesthetascs; dbs = distal burrowing spine of the antenna II basipodite; en = endopodite of the antenna II; ex = exopodite of the antenna II; lo = labral outgrowth; ODL = outer distal lobe of limb I; p = posterior side of the antennal branch; T1, T2 = thoracic limbs I and II, respectively. Scale bars: A, G, I = 20 μm; B, H, J = 10 μm; C, E–F = 2 μm; D = 50 μm.

portion bilaterally armed with long setulae (Fig. 11C). Seta 3' is similar in structure to seta 2' but 1.3 × longer (Fig. 11C, E). Setae 10–12 are similar in structure to the setae 8 and 9; setae 9–11 are subequal in size, seta 12 is slightly shorter (Fig. 11C). Seta 13 is short and thin, 0.4–0.5 × as long as seta 12, bisegmented, with a distal armature of long setulae (Fig. 11C). Seta α is 2.0 × as long as seta β (Fig. 11C). Ejector hooks and epipodite are as typical for the genus (Fig. 11A).

Thoracic limb II. Structure typical for the genus (Fig. 11F–H). Exopodite seta a is the longest and the thickest, 1.4–1.5 × as long as seta b, armed with long setulae; setae b and c are short and thin, closely spaced, covered by short setulae; seta b is 1.5 × as long as seta c (Fig. 11F). Scraping setae 1' and 2' are similar in structure, thin, moderately incurved, unilaterally armed with thin spinulae; seta 1' is 1.3–1.4 × the length of seta 2'. Scraper 3' is 0.8 × as long as the scraper 2'; scraper 3' is only slightly incurved and armed with ~15 relatively thick spinulae (Fig. 11F). Scrapers 4' and 5' are short and stout, scraper 3' 1.3–1.4 × as long as the scraper 4' and 1.5–1.6 × as long as the scraper 5'. The scrapers 4' and 5' are almost straight, armed with few (up to 12) thick spines; the distalmost spine of each scraper is the longest and the thickest (Fig. 11F). Scrapers 6'–8' are subequal in size, 0.7 × as long as the scraper 5', almost straight, armed with relatively numerous (more than 15) thin spinulae; inner scrapers have a finer armature (Fig. 11F). Posterior limb elements and gnathobase are as typical for the genus (Fig. 11G–H). Filtering comb consists of six bisegmented feather-like setae similar in length and structure (Fig. 11F, H).

Thoracic limb III. Conforms to the generic diagnosis (Fig. 11I). Seta b is 1.1–1.6 × the length of seta a, the setae are closely spaced, located on the outer side of theexopodite, bisegmented, setulose. Setae c–e are closely spaced, located at the distal exopodite portion. Seta c is slightly longer than seta a (Sc/Sa = 1.4), thin, unisegmented, armed with sparse long setulae along their entire length. Seta d is the longest, 2.8 × as long as seta a, 1.7–1.8 × as long as seta b, 1.9 × as long as seta c, 2.9 × as long as seta e. Seta d is thick, bisegmented, bilaterally armed with short setulae along its entire length. Seta e is relatively short and thick, unisegmented, slightly incurved, bilaterally armed with sparse spinulae. Inner limb portion is as typical for the genus. Setae 1' and 1 are subequal in size, short and thick, bisegmented; seta 1' is naked, seta 1 is geniculate, unilaterally armed with long setulae. Setae 2–4 are similar in structure, 0.8 × as long as seta 1', stout, bilaterally armed with long setulae along their entire length (Fig. 11I). Seta 2' is 0.4–0.5 × as long as seta 1', bisegmented, bearing short setulae (Fig. 11J). Inner part of the inner portion bears five anterior setae (3'–7') and four posterior setae (5–8). Anterior setae are bisegmented, naked, seta 3' is the shortest, 0.75 × as long as seta 4'; setae 4'–7' are subequal in size (Fig. 11J). Posterior setae 5–8 are similar in structure, bisegmented; the distal portion of each anterior seta is bilaterally armed with short setulae (Fig. 11I). Gnathobase is as typical for the genus (Fig. 11I).

Thoracic limb IV. Structure typical for the genus (Fig. 11K). Exopodite seta a is the shortest, unisegmented, armed with long setulae along its entire length; setae b and c are closely spaced, seta b is the longest, 2.7–2.8 × as long as seta a, 1.5 × as long as seta c. Seta b is unisegmented, with a bilateral armature of short setulae in its distal portion. Seta c is bisegmented, with an inflated proximal portion; seta c is armed with long sparse setulae along its entire length (Fig. 11K). Inner portion seta 1' is 1.9–2.0 × as long as setae 2'–4'; seta 1' is bisegmented, with the distal portion bearing a bilateral armature of long spinulae. Setae 2'–4' are similar in structure, short, bisegmented, with an inflated basal portion and a narrow flattened distal portion that is asymmetrically armed with long spinulae (Fig. 11K). Posterior setae 1–4 are similar in structure, short, bisegmented, with the distal segment armed with short setulae (Fig. 11K). Location of sensory elements and gnathobase structure conform to the generic diagnosis (Fig. 11K). The filtering comb comprises four setae.

Thoracic limb V. Smallest limb (Fig. 11L). Seta a is the longest, 3.9–4.0 × as long as seta 1, 2 × as long as seta 2, 3 × as long as seta 3. Seta a is bisegmented, inflated at its base, bilaterally armed with sparse

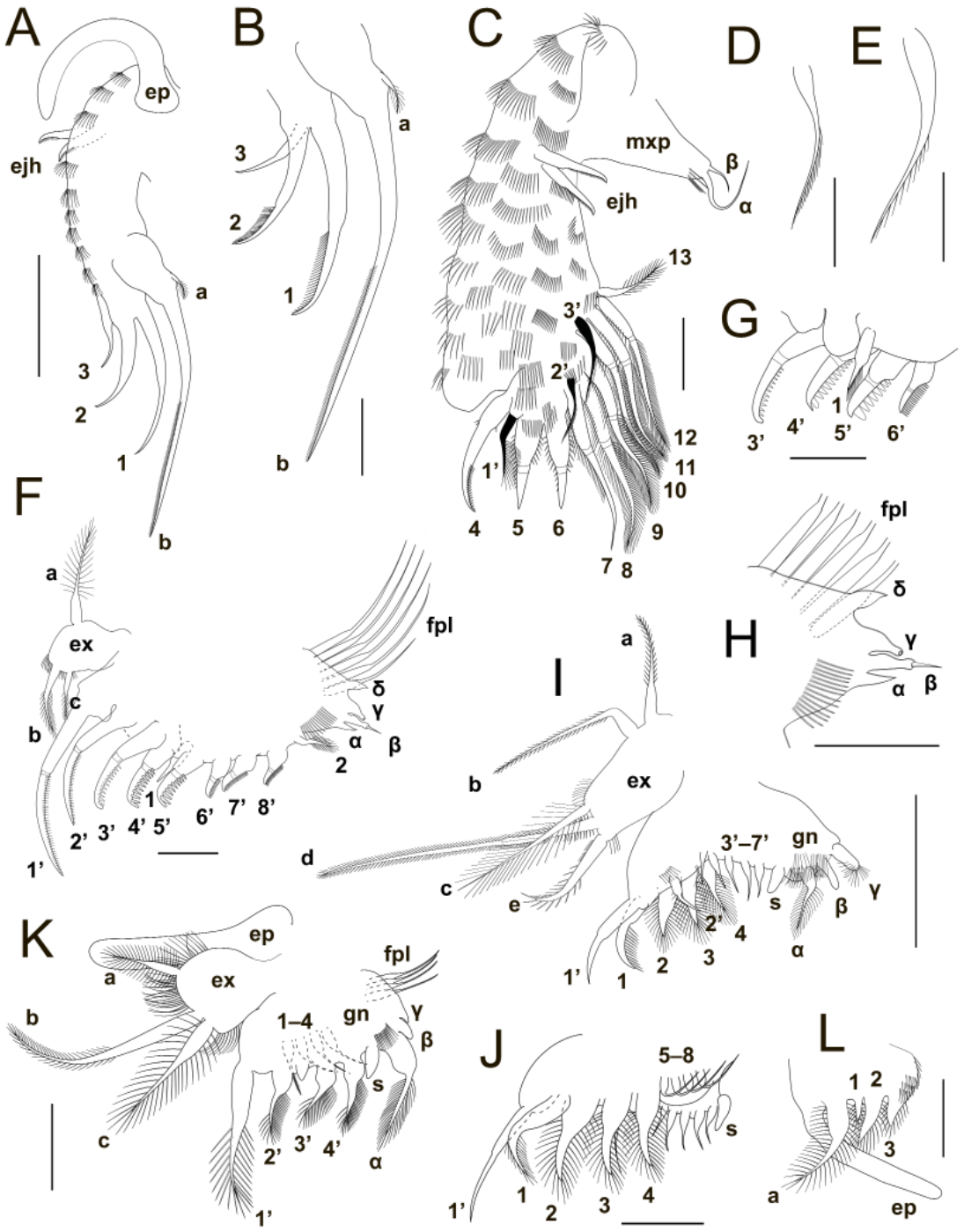

Fig. 11. *Drepanothrix asiatica* sp. nov., parthenogenetic female from the Kronotsky National Reserve, Kamchatskii Krai, Russia (MGU MI–289, type locality). **A–E**. Thoracic limb I. **A**. Outer view (inner endites are not shown). **B**. Outer limb portion (ODL and IDL). **C**. Inner endites in anterior view (ODL and IDL are not shown). **D**. Anterior seta 2'. **E**. Anterior seta 3'. **F–H**. Limb II. **F**. General anterior view. **G**. Setae of the inner limb portion, posterior view. **H**. Gnathobase in anterolateral view. **I–J**. Limb III. **I**. General anterior view. **J**. Inner endites, posterior view. **K**. Limb IV in anterior view. **L**. Limb V in anterior view. Abbreviations: ejh = ejector hooks; ep = epipodite; ex = exopodite; fpl = gnathobase filtering setae; gn = gnathobase; mxp = maxillary process of the limb I; ODL = outer distal lobe of limb I; s = sensillum. For seta labeling, see Material and methods. Scale bars: A, I = 50 μm; B–C, F–H, J–L = 20 μm; D–E = 10 μm.

setulae along its entire length (Fig. 11L). Setae of inner lobe are short, unisegmented, armed with short setulae along its entire length (Fig. 11L).

Ephippial female

Body. Length is 0.55–0.65 mm (Figs 8C–D, 12A). The body is ovoid in lateral view, flattened laterally (height : length = 0.7–0.8; width : length = 0.3–0.4). General morphology and structure of appendages are similar to those of the adult parthenogenetic female. The dorsal keel of the carapace is reduced. Dorsal valve margin is angulate in lateral view, lacking a dorsal tooth (Figs 8C–D, 12A). Valve ornamentation is similar to that of the parthenogenetic female. Ephippium is thin, transparent, lacks a well-defined ventral margin and specific sculpture, and contains two eggs (Figs 8C–D, 12A).

Male

Body. Length is 0.45–0.55 mm. The body is ovoid in lateral view, flattened laterally (height : length = 0.65–0.7; width : length = 0.3). General morphology closely resembles that of the juvenile parthenogenetic female (Figs 8E, 12B, 13A–B). The dorsal keel is well developed on both the head and carapace. The dorsal tooth is either completely absent or reduced to a low bump (Figs 8E, 12B, 13A–B). Posterodorsal angle is weakly developed or absent (Figs 12B, 13A–B). Ventral valve margin forms a wide rounded projection at the level of thoracic limb I (Figs 12C–D, 13A); the projection bears enlarged marginal teeth (Figs 12C–D), while its marginal setae are similar in length and thickness to the others (Figs 8E, 12C, 13A).

General head morphology. Similar to that of parthenogenetic female.

Thorax and abdomen. As in parthenogenetic female.

Postabdomen. Relatively small (0.3 × body length), flattened laterally (Figs 8E, 12E, 13C). Postabdomen is subtriangular in lateral view, narrowing distally (Figs 12E, 13C). The preanal angle is oblique (~150°), located at the middle of the preanal margin. The preanal margin of postabdomen is armed with 9–10 transverse rows of setulae in its proximal portion and 5–6 rows of setulae in its distal portion (Figs 12E, 13C). The lateral surface of the preanal portion bears transverse clusters of setulae, forming three longitudinal rows: ventral setulae, long anterior to the preanal angle and short posterior to the angle; medial setulae, relatively short, increasing in length towards the postabdomen base; marginal setulae, long anterior to the preanal angle and short posterior to the angle (Figs 12E, 13C). Postabdomen anal portion is relatively short, 0.25–0.3 × the length of the preanal portion. A distinct depression is present between preanal and anal margins. Anal portion bears 2–3 clusters of spines and several longitudinal groups of short setulae (Figs 12E, 13C). Postabdominal claw is relatively long and thin, 0.4 × as long as the postabdomen, 4.3–4.4 × as long as wide, slightly incurved (Figs 12E–G, 13D). Lateral claw surface bears a proximal pecten and a distal cluster of short spinulae (Fig. 12F–G); medial claw surface is armed with a cluster of short spinulae stretched along the basal and middle claw portions (Fig. 13D). Basal spine is relatively short, 0.5–0.6 × width of the claw; an additional short spine is usually located at the base of the basal spine (Figs 12F–G). Vas deferens runs along the ventral postabdomen margin, gonopore is located subterminally at the low projection (Fig. 12E).

Antenna I. Similar to that of the female in relative size and shape. An accessory seta (ms) is located at the anterior edge of the appendage. Male accessory seta is 0.8–1.0 × as long as basal sensory seta of the antenna I, slightly flattened, wide at base and narrowing distally, lacking armature (Figs 12H–I, 13E).

Antenna II. Similar to that of the female in relative size and shape but bears two additional sensory setae at the distal end of basipodite (Figs 12J, 13F–G). Distal basipodite setae are subequal in size, 1.3–1.4 × the length of the distal burrowing spine, slightly incurved, reaching distal margin of the antenna II exopodal segment 2. Both setae have a distal bilateral armature of short, thin setulae (Fig. 13G).

Labrum and mouth parts. As in parthenogenetic female.

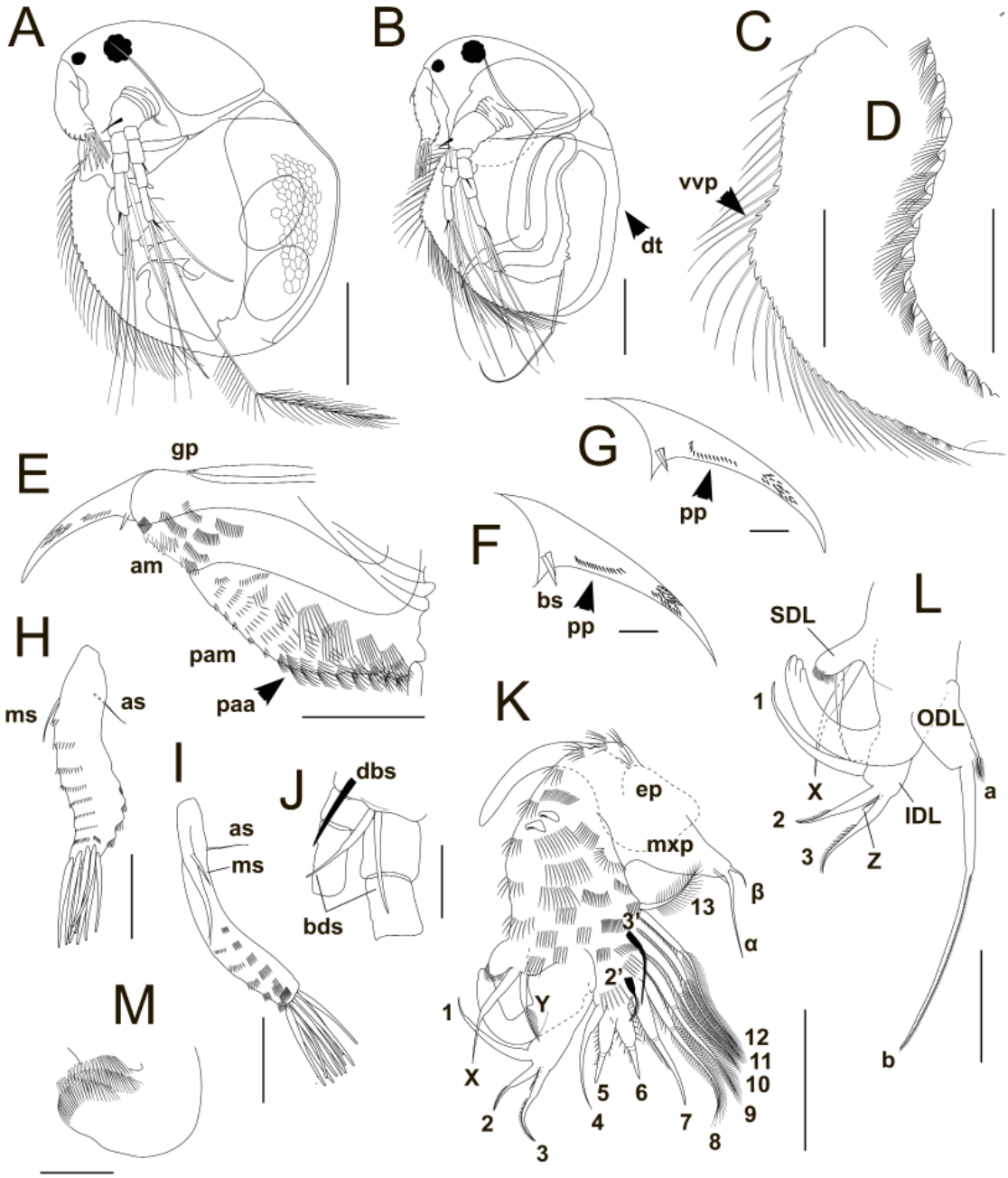

Fig. 12. *Drepanothrix asiatica* sp. nov., gamogenetic individuals from the Kronotsky National Reserve, Kamchatskii Krai, Russia (MGU MI–289, type locality). **A**. Ephippial female in lateral view. **B–M**. Male. **B**. General lateral view. **C**. Ventral valve margin. **D**. Enlarged ventral valve projection, marginal setae are not shown. **E**. Postabdomen in lateral view. **F–G**. Postabdominal claw in outer view. **H**. Antenna I in inner view. **I**. Antenna I in anterior view. **J**. Antenna II, distal armature of the basipodite. **K**. Thoracic limb I in anterior view, ODL is not shown. **L**. Limb I in outer view, inner endites are not shown. **M**. Tip of the IDL hook. Abbreviations: am = anal margin of the postabdomen; as = antennular seta; bds = distal setae of the antenna II basipodite; bs = basal spine of the postabdominal claw; dbs = distal burrowing spine of the antenna II basipodite; dt = dorsal tooth; ep = epipodite; gp = gonopore; IDL = inner distal lobe of the limb I; ms = male accessory seta of the antenna I; mxp = maxillary process of the thoracic limb I; ODL = outer distal lobe of the limb I; paa = preanal angle of postabdomen; pam = preanal margin of postabdomen; pp = proximal pecten of the postabdominal claw; SDL = subdistal lobe of the limb I; vvp = ventral valve projection. Scale bars: A–B = 200 μm; C–E, H–K = 50 μm; C, L = 100 μm; F–G = 10 μm; M = 5 μm.

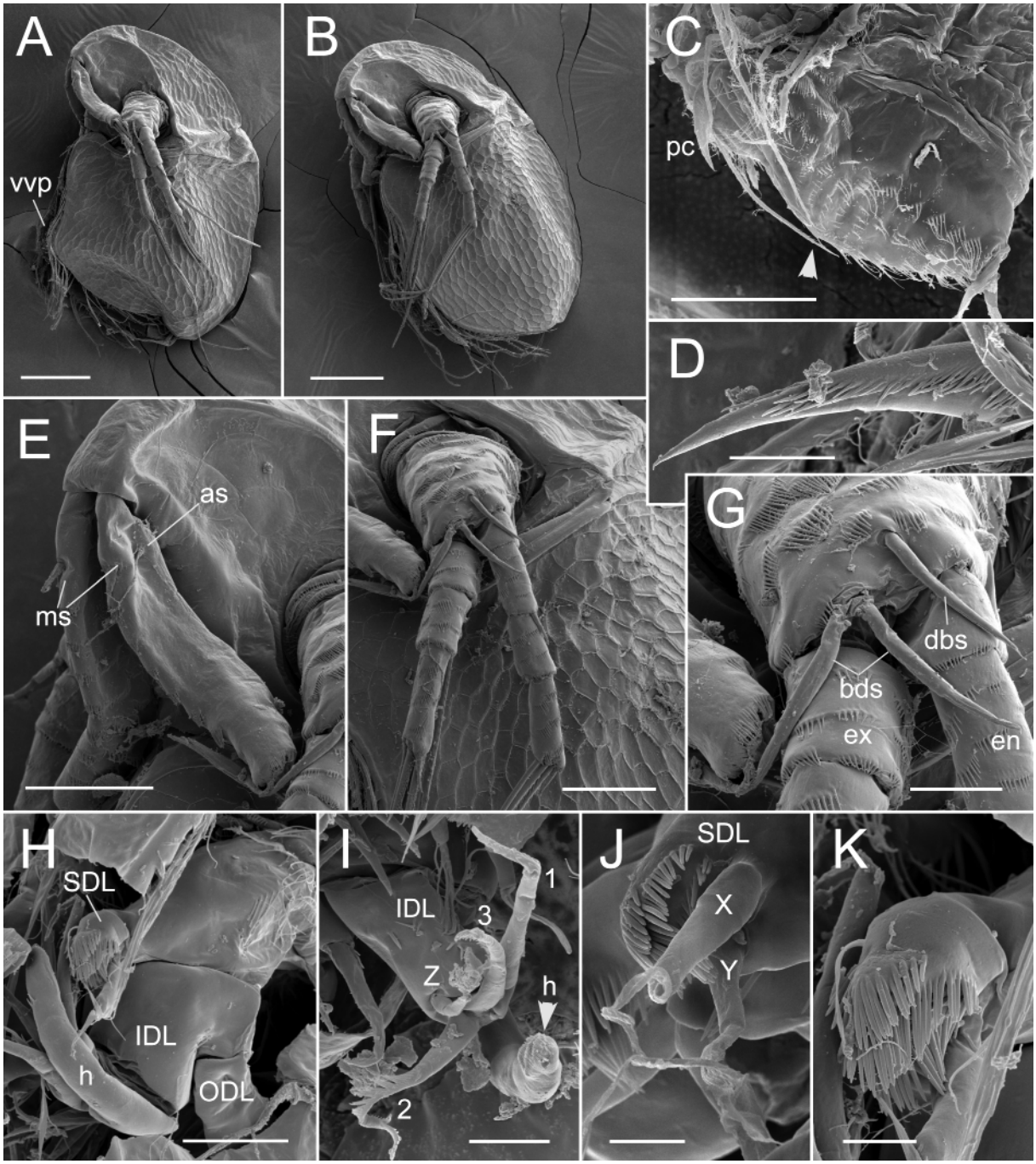

Fig. 13. Scanning electron micrographs of *Drepanothrix asiatica* sp. nov., adult male from the Kronotsky National Reserve, Kamchatskii Krai, Russia (MGU MI–289, type locality). **A–B**. General view. **C**. Postabdomen in lateral view, arrow shows oblique preanal angle. **D**. Postabdominal claw in inner view (note slender shape of the claw). **E**. Antennae I. **F**. Antenna II in lateral view. **G**. Distal armature of the antenna II basipodite. **H**. Thoracic limb I in outer view. **I**. Inner distal lobe of the limb I, inner view (white arrow indicates distal armature of the hook). **J**. Subdistal lobe in outer view. **K**. Subdistal lobe in anterior view. Abbreviations: as = sensory seta of the antenna I; bds = distal setae of the antenna II basipodite; dbs = distal spine od basipodite antenna II; en = endopodite of the antenna II; ex = exopodite of the antenna II; h = IDL hook of the thoracic limb I; IDL = inner distal lobe of the limb I; ms = male accessory seta of the antenna I; ODL = outer distal lobe of the limb I; ; pc = postabdominal claw; SDL = subdistal lobe of the limb I; vvp = ventral valve projection. Scale bars: A–B = 100 μm; C, E–F = 50 μm; D, I = 10 μm; G–H = 20 μm; J–K = 5 μm.

Thoracic limbs. Largely similar to those of the female, except for limb I.

Thoracic limb I. Largest, folded medially (Fig. 12K–L). A small rounded subdistal lobe (SDL) is located at the anteromedial limb surface, proximally to the inner distal lobe (IDL) (Figs 12K–L, 13H). The subdistal lobe is slightly flattened dorsoventrally, approximately reaching the tip of the IDL hook. The anterior surface of the SDL bears three rows of flattened spinulae and two bisegmented setae (X and Y) (Figs 12L, 13J–K). Seta X is 1.4 × as long as seta Y, naked. Seta Y has a distal unilateral armature of short setulae (Figs 12K, 13J). The outer distal lobe (ODL) bears a long thick apical seta b and a short feather-like seta a at its base, 0.15 × as long as seta b (Fig. 12L). Inner distal lobe (IDL) has a large incurved hook subdistally; the hook is cylindrical in cross-section, smooth, at most bearing few small solitary spinulae in distal portion (Fig. 13H). The hook tip is armed with three transverse rows of closely spaced, flattened spinulae (Figs 12M, 13I). Distal IDL portion bears four setae (1–3, Z). Seta 1 is the longest, 1.4 × as long as seta 2, 1.5 × as long as seta 3. Seta 1 is bisegmented, with a naked, slightly incurved basal portion 4.7 × as long as the distal portion; the distal portion is short, slightly incurved, armed with thin spinulae (Figs 12K–L, 13I). Seta 2 is long, with a distal portion exceeding in length the basal portion; seta 2 distal portion is unilaterally armed with long setulae; seta 3 is similar to seta 2 but shorter, it is located between setae 1 and 2 (Figs 12K–L, 13I). Male accessory seta (Z) is located on the anterior side of the IDL, 0.3 × as long as seta 3, naked (Figs 12K–L, 13I). Limb I inner portion has a similar structure to that of the female, but lacks seta 1' (Fig. 12K).

Differential diagnosis

Parthenogenetic females and males of *Drepanothrix asiatica* sp. nov. differ from those of *D. dentata* in the size of the dorsal tooth, well developed in *D. dentata* (Figs 1A, D, H, 2A, H) but strongly reduced to absent in *D. asiatica* (Figs 6A, C–G, 7A, 12B, 13H–L). However, gamogenetic females of both species have a reduced or absent dorsal tooth and cannot be reliably distinguished based on morphology (Figs 1E, 2F–G, 12A).

Males of *D. asiatica* sp. nov. also differ from those of *D. dentata* in postabdomen shape and armature, see below. In *D. dentata*, the postabdomen is subquadrangular in lateral view, with preanal angle approximately right, shifted towards the anal opening; the anterior part of the preanal portion is much longer than the posterior one (Figs 1I, 2J). In contrast, males of *D. asiatica* have a subtriangular postabdomen with oblique preanal angle located in the middle of the postabdomen preanal portion (Figs 12E, 13C). The shape of the postabdominal claw also differs between the two species. In *D. dentata*, the postabdominal claws are short and stout (0.3 × postabdomen length, 2.7–3.2 × as long as wide), bearing two clusters of spinulae that do not form a pecten (Figs 1J–K, 2K–L). In *D. asiatica*, the claws are relatively long and slender (0.4 × postabdomen length, 4.3–4.4 × as long as wide), with the lateral surface of the claw bearing a proximal pecten of spinulae and a distal cluster not forming a pecten (Fig. 12F–G).

The observed differences between *D. asiatica* sp. nov. and *D. dentata* are summarized in Table 2.

Remarks

The known range of *Drepanothrix asiatica* sp. nov. includes eastern and northern Kamchatka (Dadykin *et al.* 2025), Bering Island (Novichkova & Chertoprud 2015), Chukotka Peninsula (Smirnov 1976), Khabarovsk Territory, Magadan Area (Streletskaya 2010), Sakhalin Island, the Kuril Islands (Uéno 1932), and northern Japan (Inoue 1968). No populations of *Drepanothrix* were found in the Russian portion of the Amur basin (Kotov *et al*. 2011; Garibian *et al*. 2021b) or northern China (Ji *et al*. 2015). Also, a record of parthenogenetic *Drepanothrix* with a reduced dorsal tooth from Irkutsk Area (Yermolayeva & Fetter 2020: fig. 2a, c) likely refers to *D. asiatica*. This indicates that the species may be widely distributed in East Asia.

Table 2. Diagnostic features of *Drepanothrix dentata* (Eurén, 1861) and *D. asiatica* sp. nov.

Feature	***Drepanothrix dentata* (Eurén, 1861)**	***D. asiatica* sp. nov.**
dorsal tooth (parthenogenetic female, male)	large	strongly reduced or absent
preanal angle of postabdomen (male)	roughly right, shifted towards anal opening	oblique, located at the middle of preanal margin
postabdominal claw (male)	short, stout (length:width = 2.7–3.2)	long (length:width = 4.3–4.4)
lateral side of postabdominal claw (males)	two clusters of spinulae not forming a pecten	two clusters of spinulae, the proximal cluster pecteniform

Drepanothrix asiatica sp. nov. occurs in a variety of water bodies, including *Sphagnum* bogs and lakes, and slightly brackish seashore pools. The species is relatively rare and occurs on muddy sediment or plant litter in the littoral zone. The lifestyle of *D. asiatica* has not been studied so far. However, it is likely similar to its sibling species *D. dentata*, which is adapted for burrowing and detritus feeding (Fryer 1974; Kotov 2006) but also inhabits submerged macrophytes (Błędzki & Rybak 2016; Korovchinsky & Kotov 2021).

Genetic variability

We obtained 15 *COI*, 23 16S rDNA, and 7 ITS1 sequences (Supp. file 2: Table S1). We combined these data with seven sequences of the Folmer's *COI* and two of the 16S rDNA from the NCBI GenBank. Final alignment lengths were: *COI*, 629 bp; 16S rRNA, 403 bp; ITS1, 492 bp. The best-fitting model for the multigene phylogram was TPM3u+F+I. Three major phylogroups were recognized within *Drepanothrix*: European *D. dentata* s. str., East Eurasian *D. asiatica* sp. nov., and Canadian *D.* cf. *dentata* (Figs 14, 15A). Notably, macrothricid sequences available in the GenBank formed very long branches when placed as the outgroup for *Drepanothrix* (Fig. 15A). Therefore, we reconstructed the midpoint-root multigene ML phylogram (Fig. 15B) to reveal the relative position of the major clades. In this case, European and Canadian phylogroups appeared to be closer to each other than to the East Eurasian clade (Fig. 15B).

Analyses of individual gene fragments also recovered the three clades (Supp. file 1: Fig. S1), though branch support was low for the 16S rDNA tree (Supp. file 1: Fig. S1B). Distances between phylogroups revealed by *COI* barcoding were significantly higher than the intragroup variability (Fig. 16). The 16S rRNA nucleotide variability did not allow us to distinguish the phylogroups with confidence (Fig. 16; Supp. file 1: S1B), as the sequences had only 1–2% of differing sites. The ITS1 variability was also significant (Supp. file 1: Fig. S1C), but ITS1 data was available for only a few specimens, none from the Canadian clade.

Mitochondrial genomes

For both *Drepanothrix dentata* and *Macrothrix triserialis*, all the expected mitochondrial genes (13 PCGs, 2 rRNA, 22 tRNA) have been recovered. In both cases, mitogenome length is about 15 kbp, and GC content is ca 31%. Unexpectedly, the mitochondrial genomes of *D. dentata* and *M. triserialis* differ by gene order. In *D. dentata*, a non-coding region bordered by tRNA genes (a putative control region) is situated between the srRNA and lrRNA genes (Fig. 17A). In contrast, in *M. triserialis* the rRNA genes are separated only by a single tRNA (as typical for animal mitochondria), and putative control region is located after the srRNA gene (Fig. 17B). The mitogenome structure of *D. dentata* was

verified by PCR with subsequent direct sequencing of the region in another sample of *D. dentata*. The sequenced region is very similar to the assembled one and minor differences between them are expected since they are obtained from different organisms (Supp. file 3). In this respect, the unusual genome structure of *Drepanothrix* is unlikely to be a result of incorrect assembling or annotation.

The phylogenetic position of *Drepanothrix* is also surprising. Our phylogenetic analysis retained highly supported clades of Daphniidae Straus, 1820, Moinidae Goulden, 1968, Bosminidae Baird, 1845, and Chydoridae Dybowski & Grochowski, 1894 + Eurycercidae Kurz, 1875 (Fig. 18). The relative position of these clades is unresolved. *Macrothrix triserialis* is considered a sister taxon to Moinidae and forms a well-supported clade with the latter. At the same time, *D. dentata* is placed in a basal position to all other anomopods, although the support for this node is weak (Fig. 18). Therefore, Macrothricidae appears to be a non-monophyletic group according to our data.

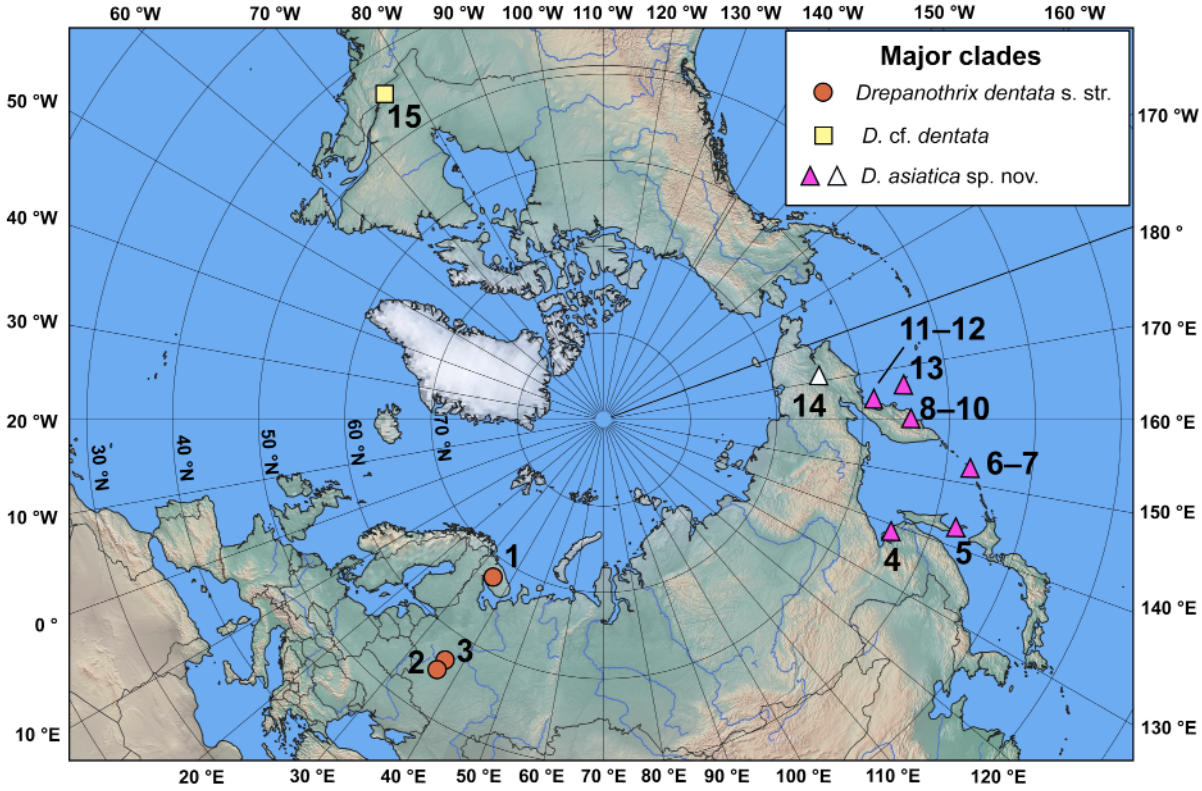

Fig. 14. Geographic location of studied *Drepanothrix* Sars, 1862 populations. Points indicate studied localities. Point shape and colour correspond to major phylogroups of *Drepanothrix*, as follows: orange circles = *D. dentata* (Eurén, 1861), yellow square = Canadian *D.* cf. *dentata*; violet triangles = *D. asiatica* sp. nov.; white triangle = *D. asiatica* sample with only morphological data available. Localities: 1. Lake Lovozero, Murmansk Area, Russia. 2. Lake Glubokoe, Moscow Area, Russia. 3. Abandoned peat mining pond near Merilovo, Tver Area, Russia. 4. Small lake in Nikolay Bay, Khabarovskii Krai, Russia. 5. Sphagmal lake near Pokrovka, Sakhalin Island, Sakhalin Area, Russia. 6–7. Small sphagnal bogs in Simushir Island, Sakhalin Area, Russia. 8–10. Small lakes in the Kronotsky Nature Reserve, Kamchatskii Krai, Russia. 11–12. Small lakes in Karaginsky Island, Kamchatskii Krai, Russia. 13. Small lake near Nikolskoe, Bering Island, Kamchatskii Krai, Russia. 14. Puddle in the vicinity of Anadyr River, Chukotskii Autonomous Region, Russia. 15. Eel Lake, Ontario, Canada. For more information on localities, see Table 1.

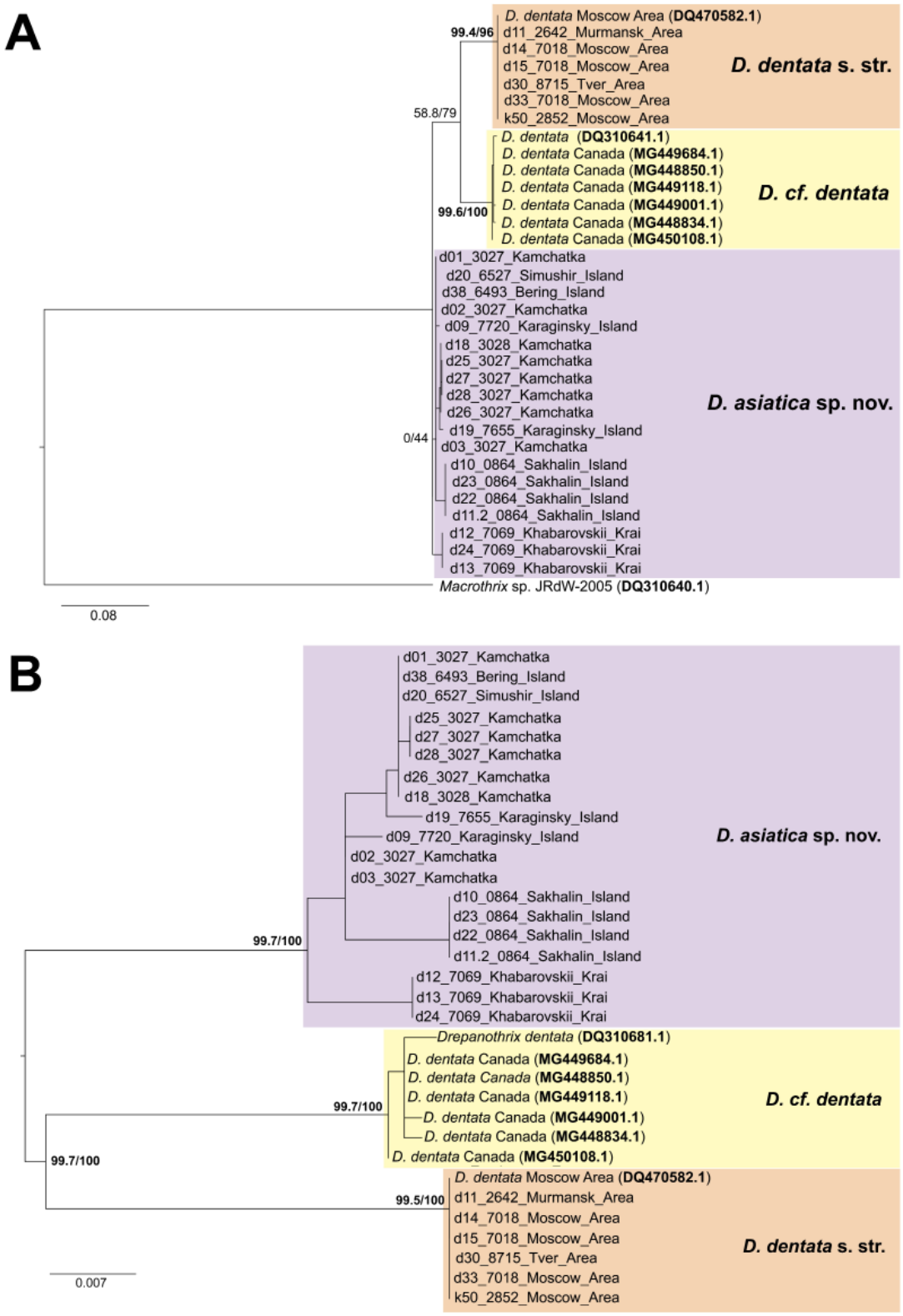

Fig. 15. Maximum likelihood phylograms based on sequences of the mitochondrial cytochrome c oxidase subunit I (COI), 16S rRNA, and nuclear ITS1. **A**. Phylogram with COI and 16S sequences of *Macrothrix* sp. (DQ310640.1, DQ310680.1) as an outgroup. **B**. Midpoint-rooted phylogram. The node support values are based on SH-aLRT/ultrafast bootstrap. Colours indicate major phylogroups.

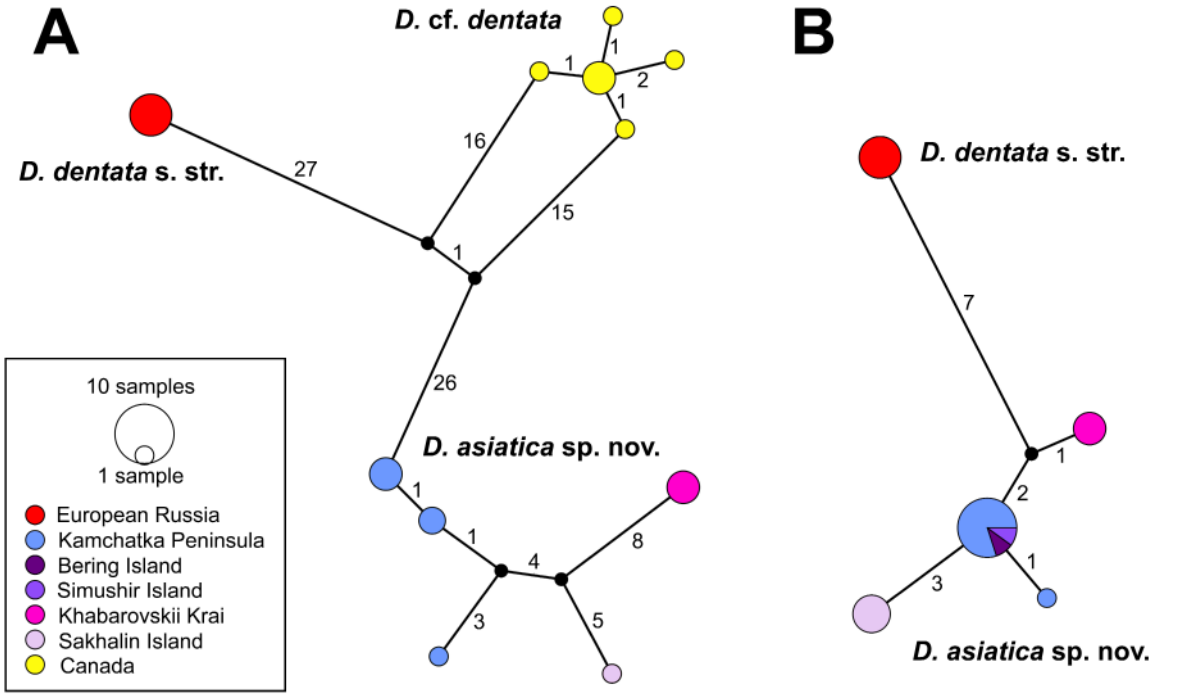

Fig. 16. TCS haplotype networks for *Drepanothrix* Sars, 1862. **A**. Folmer's *COI* gene fragment. **B**. 16S rRNA gene fragment.

Discussion

Taxonomy and biogeography of *Drepanothrix*

The morphological data presented here confirm the distinct status of *D. asiatica* sp. nov. Both parthenogenetic female and male features are suitable for distinguishing the two taxa (Table 2), while gamogenetic females lack clear diagnostic characters. The presence or absence of a dorsal tooth is the most convenient diagnostic character, especially given the rarity of males. However, this structure might play a protective role and thus develop in the presence of predator elicitors (Sperfeld *et al.* 2020), similarly to various cuticular outgrowths of *Daphnia* O.F. Müller, 1785 (Hammill *et al.* 2008; Octorina *et al.* 2022; Pereboev *et al.* 2025). Unfortunately, only a few populations of *Drepanothrix* were available for morphological analysis, and observed variation in dorsal tooth size was limited in both species. Nevertheless, absence or reduction of the structure in gamogenetic female indicates possible plasticity of this character. Therefore, male postabdomen morphology seems to be more reliable for the species identification. The observed variation between males of *D. dentata* and *D. asiatica* resembles the pattern earlier discovered in *Chydorus* Leach, 1816, in which one of two closely related species has less modified postabdomen than the other (Van Damme & Dumont 2006). As suggested for *Chydorus*, differences in postabdomen shape may mediate premating reproductive isolation (Van Damme & Dumont 2006), but this should be subject to further research.

Only a few doubtful records of *Drepanothrix* from outside the Holarctic were reported to date. First, Cornejo & Antepara (2012) recorded *D. dentata* from Lago Chongón, Guayas Province, Ecuador. However, this record clearly refers to *Grimaldina freyi* Neretina & Kotov, 2017, as is evident from the shape of the postabdomen and antenna II (Cornejo & Antepara 2012: fig. 25; Neretina & Kotov 2017). Second, Coronel *et al*. (2009) reported two ephippia of *Drepanothrix* from a peat water body in

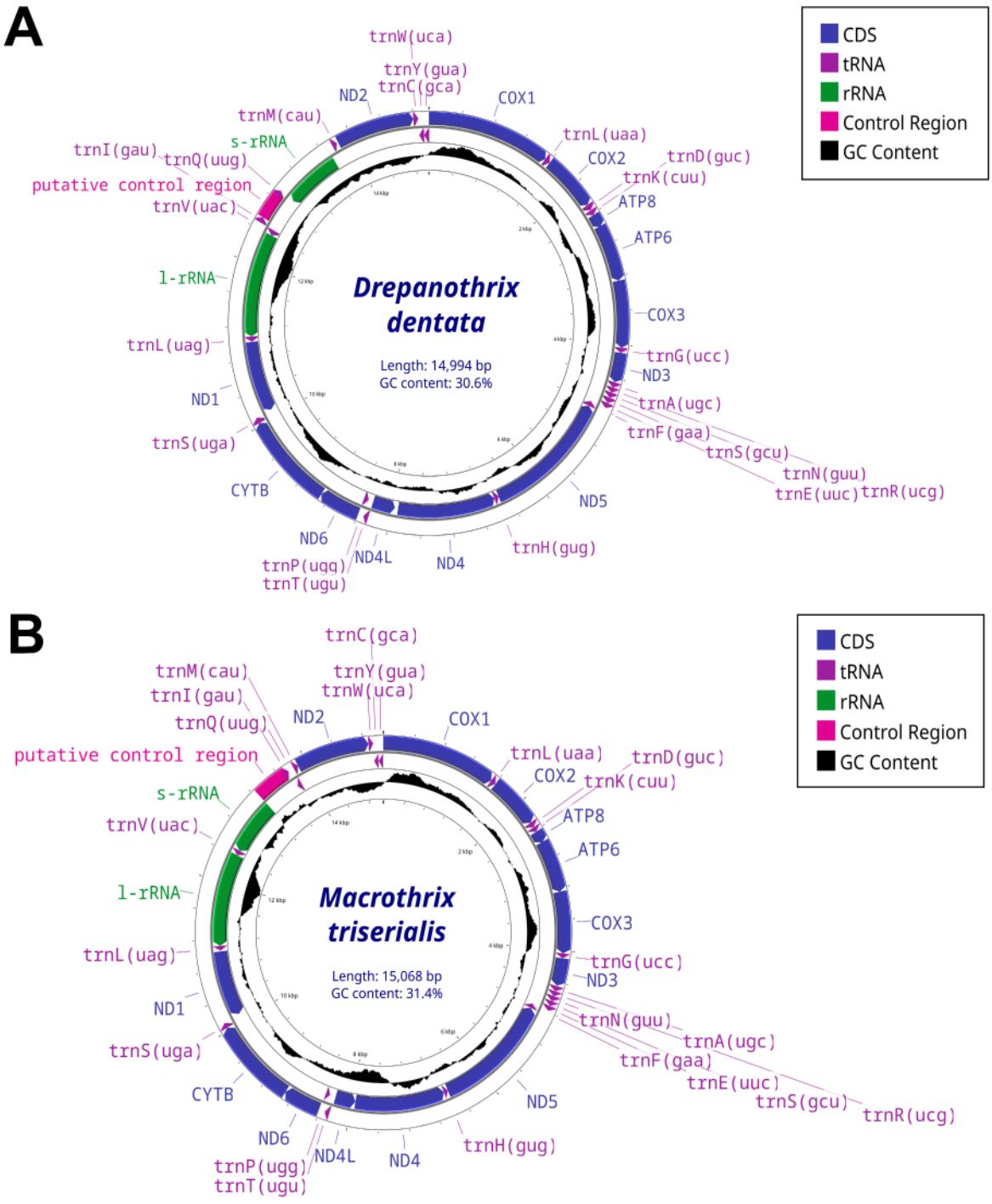

Fig. 17. Mitochondrial genome structure of two macrothricid species. **A**. *Drepanothrix dentata* (Eurén, 1861). **B**. *Macrothrix triserialis* Brady, 1886. Blue rectangles indicate protein-coding genes, purple tRNA genes, green rRNA genes, pink the putative control region. Each strand is shown separately. The black diagram in the center of the ring corresponds to the G/C content across the genome.

Cordillera del Tunari, Bolivia (Iglesias *et al*. 2016). However, the depicted ephippium (Coronel *et al*. 2009: appendix I) cannot be precisely identified by the photograph and is considerably smaller than those observed in this study (93 μm versus 330–400 μm length). Until reliable data confirms the presence of *Drepanothrix* in the Neotropics, this record should be considered a misinterpretation.

Currently, molecular markers are widely used to distinguish sibling anomopod species (Nilssen *et al.* 2007; Belyaeva & Taylor 2009; Bekker *et al.* 2016; Garibian *et al.* 2021a). In the case of *Drepanothrix*, DNA barcoding supports the results of morphological analysis and separation of Eurasian *Drepanothrix* into two major phylogroups (Figs 14–15; Supp. file 1: Fig. S1). Notably, a few Canadian *COI* sequences available in the GenBank likely belong to a separate lineage (Fig. 15; Supp. file 1: Fig. S1) which is widespread in temperate North America but occurs at a low frequency (Herrick 1884; Birge 1892; Herrick & Turner 1895; Bigelow 1922; Brooks 1959; Smirnov 1976; Smith 2001; Elías-Gutiérrez *et al.* 2018; GBIF Secretariat 2023). According to the available descriptions (Herrick & Turner 1895; Brooks 1959) and observations from iNaturalist (GBIF Secretariat 2023), the Nearctic *Drepanothrix* has a well-developed dorsal tooth, similarly to *D. dentata* s. str. Unfortunately, we had no opportunity to thoroughly revise the morphology of these populations; thus, their status requires further studies. The geographic distribution of *D. dentata* s. str. and *D. asiatica* sp. nov. in Eurasia conforms to the West Eurasian–East Asian biogeographic division previously observed in a number of anomopod genera (Kotov *et al.* 2006; Belyaeva & Taylor 2009; Jeong *et al.* 2012; Kotov *et al.* 2016, 2021; Bekker *et al.* 2018; Zuykova *et al.* 2019; Dadykin & Pereboev 2025).

General morphology and phylogenetic position of *Drepanothrix*

Despite numerous studies of parthenogenetic females in *Drepanothrix*, inaccuracies in some earlier work complicate the interpretation of several morphological characters in this genus. For instance, Alonso (1996) depicted a filtering seta on the gnathobase of thoracic limb III in *Drepanothrix dentata* (Alonso 1996: fig. 103). However, this structure was not observed in any specimens of *D. dentata* or *D. asiatica* sp. nov. studied herein (Figs 5F, 11I). Dumont & Silva-Briano (1998) mentioned the presence of a single seta on the gnathobase (maxillary process) of thoracic limb I, but in fact the maxillary process bears two setae (Figs 11C, 12K). Korovchinsky & Kotov (2021) described a dorsal organ of *D. dentata* as a 'fenestra' of thin cuticle surrounded by a cuticular ring but did not mention a conical shape of the organ. Dadykin *et al.* (2025) provided a preliminary description of *D. asiatica* from Karaginsky Island, northeastern Kamchatka, and noted the shortened apical segment of the postabdominal seta, which was similar to that of some *Macrothrix* species (Dumont *et al.* 2002). In fact, the authors provided a micrograph of a damaged seta (Dadykin *et al.* 2025: fig. S1f), which is a common artifact in ethanol-preserved material. These inaccuracies could hamper phylogenetic placement of *Drepanothrix* in previous research which was based on morphological characters only (Dumont & Silva-Briano 1998; Elmoor-Loureiro 2005).

In this study, we provide the first detailed description of male morphology in *Drepanothrix*. Males can be distinguished from parthenogenetic females by a different shape of valve and postabdomen. Also, male morphological traits include presence of additional setae on the antenna I and the basipodite of antenna II, and a specific structure of the thoracic limb I. Some of male features might be significant for understanding phylogeny of Macrothricidae. For instance, additional setae of male antenna II are present in *Grimaldina* Richard, 1892 (Kořínek, 1984), *Guernella* Richard, 1892, and *Lathonura* Lilljeborg, 1853 (Dadykin & Pereboev 2025). However, this character is not found in 'true macrothricids' of the subfamily Macrothricinae Dumont & Silva-Briano, 1998: *Macrothrix*, *Bunops*, *Wlassiczia*, and *Streblocerus* (Smirnov 1976; Silva-Briano & Dumont 2001; Dumont *et al.* 2002; Martinez-Caballero *et al.* 2017). Another feature of *Drepanothrix*, a subdistal lobe present on male limb I is also observed in *Guernella*, *Lathonura*, *Macrothrix tripectinata* Weisig, 1934, and *Pseudomoina* Sars, 1912 (Smirnov 1976; Kořínek 1984; Kotov 1999; Dadykin & Pereboev 2025). Earlier, Dumont & Silva-Briano

(1998) and Elmoor-Loureiro (2005) suggested a close relationship between *Lathonura*, *Pseudomoina*, and *Guernella*. However, their morphological analysis did not support a close relationship between *Macrothrix* and *Drepanothrix*, and the remaining genera suggesting this feature could be homoplastic rather than synapomorphic.

Dumont & Silva-Briano (1998) proposed the subfamily Macrothricinae based on the following characters: 1) anterior setae of thoracic limb I endites 2 and 3 are forked; 2) thoracic limb V exopodite and endopodite are incompletely fused; 3) mid-dorsal zone of postabdomen bears a transverse rows of spines. In *Drepanothrix*, however, the anterior setae of thoracic limb I endites 2 and 3 lack Fryer's fork (Figs 5A–C, 11C–E), and the exopodite and endopodite of limb V appear completely fused (Figs 5J, 11L). According to Elmoor-Loureiro (2005), the subfamily is characterized by the following synapomorphies: 1) at least some of the thoracic limb I anterior setae are forked; 2) anterior seta of thoracic limb I endite 2 is present; 3) limb II gnathobase filtering comb consists of 4–5 setae; 4) postabdomen marginal denticles form transverse rows. Again, no fork-like setae are present on limb I of *Drepanothrix*. Also, the

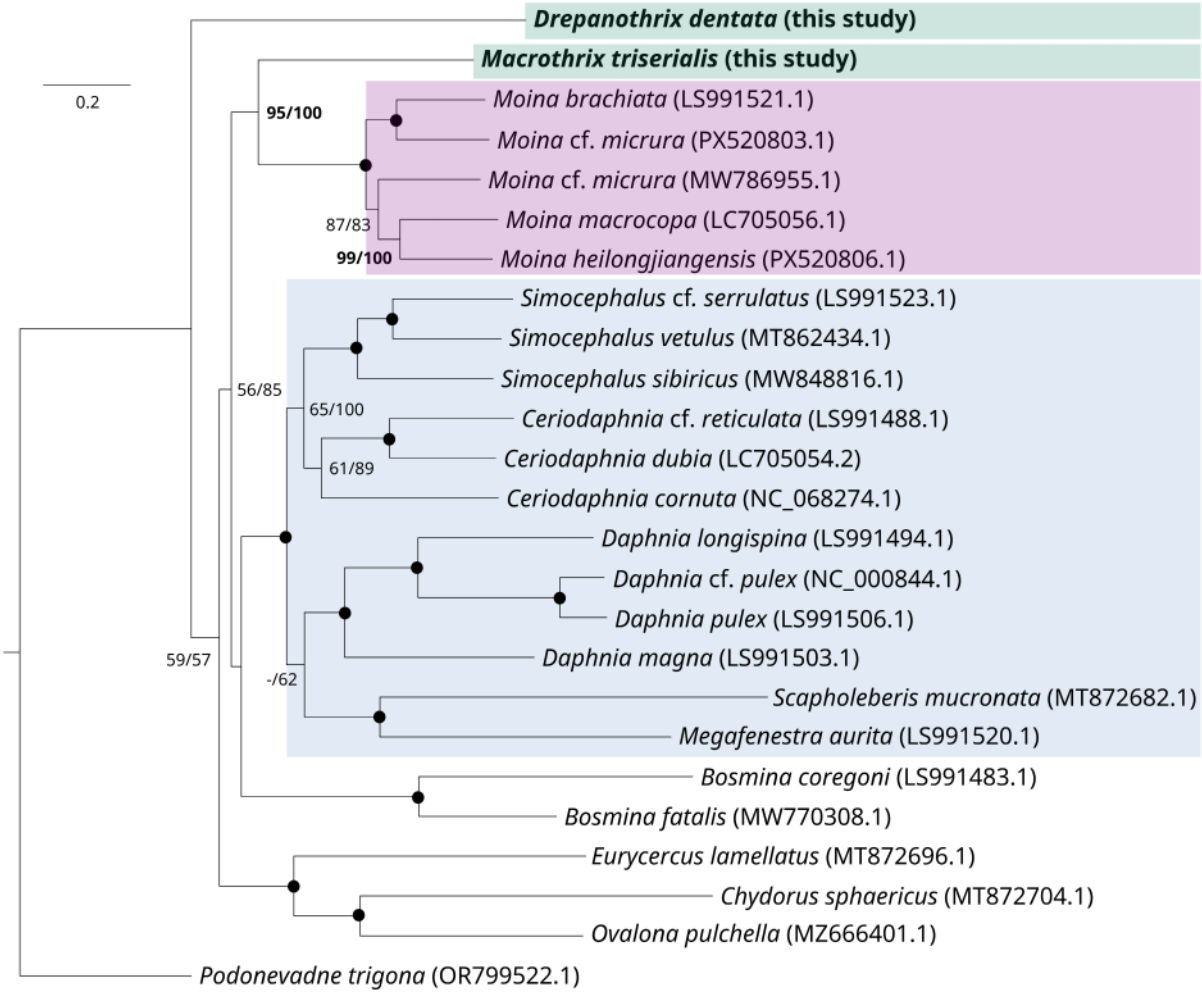

Fig. 18. Mitogenome-based maximum likelihood phylogram of Anomopoda Sars, 1865. Ultrafast bootstrap/SH-aLRT supports are given at the nodes, supports higher than or equal to 95/80 are highlighted in bold, only supports > 50 are shown. Nodes with the maximal supports are indicated by black circles. Original samples are highlighted in bold. Colored rectangles encompass representatives of families Daphniidae, Moinidae, and Macrothricidae.

limb II gnathobase filtering comb consists of six setae (Fig. 11F, H), a feature shared with *Grimaldina* only (Neretina & Kotov 2017: fig. 5c–d). Moreover, *Drepanothrix* is unique in having three setae at the thoracic limb II exopodite (Figs 5D, 11I), in contrast with 0–2 in other macrothricids and a single seta present in Macrothricinae (Dumont & Silva-Briano 1998). Thus, the placement of *Drepanothrix* in Macrothricinae is questionable, although the genus shares many features with the other macrothricines (Dumont & Silva-Briano 1998; Elmoor-Loureiro 2005).

The morphological affinities of *Drepanothrix* fit the molecular results. Our phylogenetic analysis (Fig. 18) agrees with the available genomic studies and retains the clades of Daphniidae, Moinidae, and Eurycercoidea (Xu *et al*. 2021; Van Damme *et al*. 2022). The phylogenetic position of *Macrothrix triserialis* also confirms the results of previous studies which considered Macrothricidae a sister group for Moinidae (Xu *et al*. 2021; Van Damme *et al*. 2022) or Daphniidae (Righetti *et al*. 2025). However, *Drepanothrix* appears to be distant from *Macrothrix* (Fig. 18).

This result is supported by a mitogenome structure of *Drepanothrix* atypical for crustaceans and unique at least in Branchiopoda (Fig. 17). Earlier, mitochondrial gene order rearrangements have been reported for different lineages within Cladocera (Castellucci *et al*. 2022). However, none of them displayed a location of the control region similar to that of *Drepanothrix*. In this respect, we can assume that *Drepanothrix* is not a close relative of Macrothricinae (including *Macrothrix triserialis*). While macrothricines are indeed relatives of Daphniidae and Moinidae, *Drepanothrix* might represent a basal lineage of Anomopoda. Therefore, the family Macrothricidae should be considered non-monophyletic, as was suggested earlier (Elmoor-Loureiro 2004). Nevertheless, the relative position of *Drepanothrix* and 'non-macrothricines' sensu Dumont & Silva-Briano (1998) is still unclear, as genomic data have not yet been obtained for the latter.

Our study is among the pioneer works to understand the position and composition of the macrothricid-like anomopods based on genomic methods. Apparently, we are only at the starting point, and we are planning to continue such efforts. We hope that in the future including a wider subset of Anomopoda to the analysis will clarify relationships within the family Macrothricidae and establish the phylogenetic position of *Drepanothrix* more certainly.

Acknowledgements

We are deeply grateful to V.R. Alekseev, N.M. Sukhikh, and E.A. Musatkina for the access to the collections of the Zoological Museum of the St Petersburg State University, Saint Petersburg, Russia and the Zoological Museum of the MSU, Moscow, Russia. We express a particular gratitude to the collectors of the material: S. Bakhmarin, E.I. Bekker, P.G. Garibian, M.O. Ivanova, F.V. Kazansky, N.M. Korovchinsky, A.A. Kotov, O. Krylovich, E. Kuzmicheva, A.N. Reshetnikov, O. Shpak, O. Smyshliaeva, and P.V. Volkova. We appreciate valuable comments of A.A. Kotov and P.G. Garibian (IEE RAS) that significantly improved the quality of this study. Many thanks to A.A. Kotov for editing the text. The scanning electron microscopy was conducted using Joint Usage Center "Instrumental Methods in Ecology" at the A.N. Severtsov Institute of Ecology and Evolution of the Russian Academy of Science, Moscow, Russia (head of the department R.M. Khatsaeva). A piece of material was collected at the "Glubokoe Lake" Biological Station (head Dr N.M. Korovchinsky), and we are very grateful to its staff for their help with logistics and sample collecting. The study is supported by the Russian Science Foundation (grant No 25-74-00070).

Data availability

All studied samples were deposited to a working collection of the Laboratory of aquatic ecology and invasions of A.N. Severtsov Institute of Ecology and Evolution of the Russian Academy of Sciences,

Moscow, Russia) (IEE AAK). Type material is deposited in the collection of the Zoological Museum of the Moscow State University, Moscow, Russia (access numbers MGU MI–287–MGU MI–289) and in the collection of the Zoological Museum of the Zoological Institute of the Russian Academy of Sciences, Saint Petersburg, Russia (access numbers ZIN 55222–ZIN 55224). The original sequences were submitted to NCBI GenBank (access numbers PZ382538–PZ382539, PZ391973–PZ391986, PZ394653–PZ394682) (Supp. file 2: Table S1).

References

Alekseev V.R. & Tsalolikhin S.Y. (eds). 2010. *A Keybook for Zooplankton and Zoobenthos of Fresh Waters of European Russia. Vol. 1. Zooplankton*. KMK Scientific Press, Moscow, Saint Petersburg. [In Russian.]

Alonso M. 1996. *Crustacea, Branchiopoda. Fauna Iberica, V. 7*. Museo Nacional de Ciencias Naturales Consejo Superior de Investigaciones Cientificas, Madrid.

Behning A.L. 1947. Cladocera of the Caucasus. Gruzmedgiz, Tbilisi. [In Russian.]

Bekker E.I., Karabanov D.P., Galimov Y.R. & Kotov A.A. 2016. DNA barcoding reveals high cryptic diversity in the North Eurasian *Moina* species (Crustacea: Cladocera). *PLoS ONE* 11 (8): e0161737. https://doi.org/10.1371/journal.pone.0161737

Bekker E.I., Karabanov D.P., Galimov Y.R., Haag C.R., Neretina T.V. & Kotov A.A. 2018. Phylogeography of *Daphnia magna* Straus (Crustacea: Cladocera) in Northern Eurasia: Evidence for a deep longitudinal split between mitochondrial lineages. *PLoS ONE* 13 (3): e0194045. https://doi.org/10.1371/journal.pone.0194045

Belyaeva M. & Taylor D.J. 2009. Cryptic species within the *Chydorus sphaericus* species complex (Crustacea: Cladocera) revealed by molecular markers and sexual stage morphology. *Molecular Phylogenetics and Evolution* 50 (3): 534–546. https://doi.org/10.1016/j.ympev.2008.11.007

Berg K. 1929–1930. A faunistic and biological study of Danish Cladocera. *Videnskabelige Meddelelser fra Dansk Naturhistorisk Forening i Kjøbenhavn* 88: 31–112.

Bigelow N.K. 1922. Representative Cladocera of South-Western Ontario. *University of Toronto Studies. Publications of the Ontario Fisheries Research Laboratory* 8: 109–126.

Birge E.A. 1892. List of Crustacea Cladocera from Madison, Wisconsin. *Transactions of the Wisconsin Academy of Sciences, Arts and Letters* 8: 379–398.

Birge E.A. 1918. The water fleas (Cladocera). *In*: Ward H.B. & Whipple G.Ch. (eds) *Fresh-Water Biology*. Wiley & Sons Inc., New York.

Błedzki L.A. & Rybak J.I. 2016. *Freshwater Crustacean Zooplankton of Europe. Cladocera & Copepoda (Calanoida, Cyclopoida). Cladocera & Copepoda (Calanoida, Cyclopoida) Key to Species Identification, with Notes on Ecology, Distribution, Methods and Introduction to Data Analysis*. Springer, Cham. https://doi.org/10.1007/978-3-319-29871-9

Boratyn G.M., Camacho C., Cooper P.S., Coulouris G., Fong A., Ma N., Madden T.L., Matten W.T., McGinnis S.D., Merezhuk Y., Raytselis Y., Sayers E.W., Tao T., Ye J. & Zaretskaya I. 2013. BLAST: A more efficient report with usability improvements. *Nucleic Acids Research* 41 (W1): W29–W33. https://doi.org/10.1093/nar/gkt282

Brooks J.L. 1959. Cladocera. *In*: Edmondson W.T. (ed.) *Ward & Whipple Fresh-Water Biology, 1st Edition*. Wiley, New York.

Capella-Gutiérrez S., Silla-Martínez J.M. & Gabaldón T. 2009. trimAl: a tool for automated alignment trimming in large-scale phylogenetic analyses. *Bioinformatics* 25 (15): 1972–1973. https://doi.org/10.1093/bioinformatics/btp348

Castellucci F., Luchetti A. & Mantovani B. 2022. Exploring mitogenome evolution in Branchiopoda (Crustacea) lineages reveals gene order rearrangements in Cladocera. *Scientific Reports* 12 (1): e4931. https://doi.org/10.1038/s41598-022-08873-y

Chen S. 2023. Ultrafast one-pass FASTQ data preprocessing, quality control, and deduplication using fastp. *iMeta* 2 (2): e107. https://doi.org/10.1002/imt2.107

Chernomor O., von Haeseler A. & Minh B.Q. 2016. Terrace aware data structure for phylogenomic inference from supermatrices. *Systematic Biology* 65 (5): 997–1008. https://doi.org/10.1093/sysbio/syw037

Clement M., Snell Q., Walker P., Posada D. & Crandall K. 2002. TCS: estimating gene genealogies. *In*: *Proceedings of the 16th International Parallel and Distributed Processing Symposium* 3: 184. Institute of Electrical and Electronics Engineers, Ft. Lauderdale. https://doi.org/10.1109/IPDPS.2002

Cornejo C.I.B. & Antepara M.C. 2012. Preliminary study of the diversity of Cladocera in Lake Chongón, Guayas. *Revista Científica Ciencias Naturales y Ambientales* 6 (1): 35–52. [In Spanish.] https://doi.org/10.53591/cna.v6i1.200

Coronel J.S., Aguilera X., Deckeck S. & Brendonck L. 2009. Resting egg bank reveals high cladoceran species richness in high-altitude temporary peat land pools. *Revista Boliviana de Ecología y Conservación Ambiental* 25: 51–67.

Dadykin I.A. & Pereboev D.D. 2025. Revision of *Lathonura rectirostris* (OF Müller, 1785) (Anomopoda, Macrothricidae) leads to translocation of East Asian populations to a separate species, *Lathonura bekkerae* sp. nov. *ZooKeys* 1249: 147–192. https://doi.org/10.3897/zookeys.1249.154922

Dadykin I.A., Volkova P.A., Ivanova M.O., Novichkova A.A. & Chertoprud E.S. 2025. Filling the gaps: diversity of the freshwater microcrustaceans of Karaginsky Island (Kamchatka, Northwest Pacific). *Limnology* 26: 195–210. https://doi.org/10.1007/s10201-024-00770-9

Dumont H.J. & Negrea S.V. 2002. Introduction to the Class Branchiopoda. *In*: *Guides to the Identification of the Microinvertebrates of the Continental Waters of the World 19*. Backhuys Publishers, Leiden.

Dumont H.J. & Silva-Briano M. 1998. A reclassification of the anomopod families Macrothricidae and Chydoridae, with the creation of a new suborder, the Radopoda (Crustacea: Branchiopoda). *Hydrobiologia* 384: 119–149. https://doi.org/10.1023/A:1003259630312

Dumont H.J., Briano M.S. & Subhash Babu K.K. 2002. A re-evaluation of the *Macrothrix rosea-triserialis* group, with the description of two new species (Crustacea Anomopoda: Macrothricidae). *Hydrobiologia* 467: 1–44. https://doi.org/10.1023/A:1014933227259

Elías-Gutiérrez M., Valdez-Moreno M., Topan J., Young M.R. & Cohuo-Colli J.A. 2018. Improved protocols to accelerate the assembly of DNA barcode reference libraries for freshwater zooplankton. *Ecology and Evolution* 8 (5): 3002–3018. https://doi.org/10.1002/ece3.3742

Elmoor-Loureiro L.M. 2004. Phylogenetic relationships among families of the order Anomopoda (Crustacea, Branchiopoda, Cladocera). *Zootaxa* 760 (1): 1–26. https://doi.org/10.11646/zootaxa.760.1.1

Elmoor-Loureiro L.M.A. 2005. A cladistic analysis of the genera of Macrothricidae Norman & Brady (Crustacea, Cladocera, Radopoda). *Revista Brasileira de Zoologia* 22 (3): 735–741. https://doi.org/10.1590/S0101-81752005000300034

Eurén H.A. 1861. Om märkliga Crustaceer af ordningen Cladocera, funna i Dalarne. *Öfversigt af Kongligens Vetenskaps Akademiens Förhandlingar* 18: 115–118.

Flössner D. 1972. *Krebstiere, Crustacea (Kiemen- und Blattfüßer, Branchiopoda, Fischläuse, Branchiura). Die Tierwelt Deutschlands, V. 60*. Magnus Poser, Jena.

Frey D.G. 1982. Questions concerning cosmopolitanism in Cladocera. *Archiv für Hydrobiologie* 93: 484–502.

Frey D.G. 1988. Are there tropicopolitan macrothricid Cladocera? *Acta Limnologica Brasiliensia* 2: 513–525.

Fryer G. 1974. Evolution and adaptive radiation in the Macrothricidae (Crustacea: Cladocera): a study in comparative functional morphology and ecology. *Philosophical Transactions of the Royal Society of London. Series B, Biological Sciences* 269 (898): 137–274. https://doi.org/10.1098/rstb.1974.0044

Garibian P.G., Karabanov D.P., Neretina A.N., Taylor D.J. & Kotov A.A. 2021a. *Bosminopsis deitersi* (Crustacea: Cladocera) as an ancient species group: a revision. *PeerJ* 9: e11310. https://doi.org/10.7717/peerj.11310

Garibian P.G., Neretina A.N., Korovchinsky N.M., Sinev A.Y., Tchabovsky A.V., Kotov A.A. & Smirnov N.N. 2021b. The southern part of Russian Far East and Korean Peninsula as a transition zone between the boreal and tropical faunas of the waterfleas (Cladocera, Crustacea). *Zoologicheskiy Zhurnal* 99 (10): 1094–1109. [In Russian.]

GBIF Secretariat 2023. *Drepanothrix dentata* (Eurén, 1861). GBIF Backbone Taxonomy. Checklist dataset. https://doi.org/10.15468/39omei

Grant J.R., Enns E., Marinier E., Mandal A., Herman E.K., Chen C.Y., Graham M., Van Domselaar G. & Stothard P. 2023. Proksee: in-depth characterization and visualization of bacterial genomes. *Nucleic Acids Research* 51 (W1): W484–W492. https://doi.org/10.1093/nar/gkad326

Growns I., Ryder D. & Frost L. 2020. The basal food sources for Murray cod (*Maccullochella peelii*) in wetland mesocosms. *Journal of Freshwater Ecology* 35 (1): 235–254. https://doi.org/10.1080/02705060.2020.1779140

Guindon S., Dufayard J.F., Lefort V., Anisimova M., Hordijk W. & Gascuel O. 2010. New algorithms and methods to estimate maximum-likelihood phylogenies: assessing the performance of PhyML 3.0. *Systematic Biology* 59 (3): 307–321. https://doi.org/10.1093/sysbio/syq010

Hammill E., Rogers A. & Beckerman A. P. 2008. Costs, benefits and the evolution of inducible defences: a case study with *Daphnia pulex*. *Journal of Evolutionary Biology* 21 (3): 705–715. https://doi.org/10.1111/j.1420-9101.2008.01520.x

Herr O. 1913. *Drepanothrix dentata* (Eurén) in der Oberlausitz. *Archiv für Hydrobiologie* 8: 419–431.

Herr O. 1917. Die Phyllopodenfauna der preusssischen Oberlausitz und der benachbarten Gebiete. *Abhandlungen der Naturforschenden Gesellschaft zu Görlitz* 28: 1–162.

Herrick C.L. 1884. A final report on the Crustacea of Minnesota included in the orders Cladocera and Copepoda, together with a synopsis of the described species in North America, and keys to the known species of the more important genera. *In*: Winchell N.H. (ed.) *The Geological and Natural History Survey of Minnesota*: 1–191. Johnson, Smith & Harrison, Minneapolis. https://doi.org/10.5962/bhl.title.3981

Herrick C.L. & Turner C.H. 1895. Synopsis of the Entomostraca of Minnesota with descriptions of related species comprising all known forms from the United States included in the orders Copepoda, Cladocera, Ostracoda. Order Cladocera—part II. *In*: Nachtrieb H.F. (ed.) *Report of the State Zoologist for 1893 and 1894*: 141–264. The Pioneer Press Company, St. Paul.

Hoang D.T., Chernomor O., von Haeseler A., Minh B.Q. & Le Vinh S. 2018. UFBoot2: Improving the ultrafast bootstrap approximation. *Molecular Biology and Evolution* 35: 518–522. https://doi.org/10.1093/molbev/msx281

Hollwedel W. 1953. Die Wasserflöhe (Cladoceren) des Säger Meeres. *Beiträge zur Naturkunde Niedersachsens* 6 (2): 46–56.

Hudec I. 2010. *Anomopoda, Ctenopoda, Haplopoda, Onychopoda (Crustacea, Branchiopoda). Fauna Slovenska, Vol. 3*. VEDA, Bratislava. [In Slovakian.]

Ibrasheva S.I. & Smirnova V.A. 1983. Cladocera of Kazakhstan. Mektep, Almaty. [In Russian.]

Iglesias C., Bonecker C., Brandao L., Crispim M. C., Eskinazi-Sant'Anna E.M., Gerhard M., Portinho J.L., Maia-Barbosa P., Panarelli E. & Santangelo J.M. 2016. Current knowledge of South American cladoceran diapause: a brief review. *International Review of Hydrobiology* 101 (3–4): 91–104. https://doi.org/10.1002/iroh.201501825

Inoue S. 1968. Copepoda and Cladocera in the Uryu-numa moor, Hokkaido. *Japanese Journal of Limnology* 29: 148–155. [In Japanese.] https://doi.org/10.3739/rikusui.29.4_148

Jeong H.G., Kotov A.A. & Lee W. 2012. A new species of the genus *Ilyocryptus* Sars, 1862 (Cladocera: Anomopoda: Ilyocryptidae) from the East Asian Palaearctic. *Zootaxa* 3475 (1): 36–44. https://doi.org/10.11646/zootaxa.3475.1.3

Ji G.H., Xiang X.F., Chen S.Z., Yu G.L., Kotov A.A. & Dumont H.J. 2015. Annotated checklist of Chinese Cladocera (Crustacea: Branchiopoda). Part II. Order Anomopoda (families Macrotrichidae, Eurycercidae and Chydoridae). *Zootaxa* 4044 (2): 241–269. https://doi.org/10.11646/zootaxa.4044.2.4

Jiménez-Velásquez C., Atencio-Garcia V., Ayazo-Genes J.E., Espinosa-Araujo J. & Prieto-Guevara M. 2021. Management of the first feeding of dorada *Brycon sinuensis* with two species of cladocerans. *Applied Sciences* 11 (20): 9379. https://doi.org/10.3390/app11209379

Jin J.J., Yu W.B., Yang J.B., Song Y., de Pamphilis C.W., Yi T.S. & Li D.J. 2020. GetOrganelle: a fast and versatile toolkit for accurate de novo assembly of organelle genomes. *Genome Biology* 21: e241. https://doi.org/10.1186/s13059-020-02154-5

Kalyaanamoorthy S., Minh B.Q., Wong T.K.F., von Haeseler A. & Jermiin L.S. 2017. ModelFinder: fast model selection for accurate phylogenetic estimates. *Nature Methods* 14: 587–589. https://doi.org/10.1038/nmeth.4285

Katoh K. & Standley D.M. 2013. MAFFT multiple sequence alignment software version 7: Improvements in performance and usability. *Molecular Biology and Evolution* 30: 772–780. https://doi.org/10.1093/molbev/mst010

Keilhack L. 1909. Phyllopoda. *In*: A. Brauers (ed.) Die Süsswasserfauna Deutschlands. Verlag von Gustav Fischer, Jena.

Kořínek V. 1984. Cladocera. Hydrobiological Survey of Lake Bangweulu and Luapulu River Basin. *Journal of Symoens Cercle Hydrobiologique de Bruxelles* 13 (2): 1–117.

Korovchinsky N.M. & Kotov A.A. (eds). 2021. *Water Fleas (Crustacea: Cladocera) of North Eurasia. Vol. 2.* KMK Scientific Press, Moscow. [In Russian.]

Kotov A.A. 1999. Redescription of *Macrothrix tripectinata* Weisig, 1934 (Anomopoda, Branchiopoda), with a discussion of some features rarely used in the systematics of the genus. *Hydrobiologia* 403: 63–80. https://doi.org/10.1023/A:1003714909471

Kotov A.A. 2006. Adaptations of Anomopoda crustaceans (Cladocera) to the benthic mode of life. *Entomological Review* 86 (Suppl 2): S210–S225. https://doi.org/10.1134/S0013873806110157

Kotov A.A. 2013. *Morphology and Phylogeny of the Anomopoda (Crustacea: Cladocera)*. KMK Scientific Press, Moscow. [In Russian.]

Kotov A.A. & Štifter P. 2006. *Cladocera: Family Ilyocryptidae (Branchiopoda: Cladocera: Anomopoda)*. Kenobi Productions, Leiden & Backhuys, Leiden.

Kotov A.A., Ishida S. & Taylor D.J. 2006. A new species in the *Daphnia curvirostris* (Crustacea: Cladocera) complex from the eastern Palearctic with molecular phylogenetic evidence for the independent origin of neckteeth. *Journal of Plankton Research* 28 (11): 1067–1079. https://doi.org/10.1093/plankt/fbl041

Kotov A.A., Korovchinsky N.M., Sinev A.Y. & Smirnov N.N. 2011. Cladocera (Crustacea, Branchiopoda) of the Zeya River basin (Amurskaya Area, Russian Federation). 3. Systematic-faunistic and zoogeographic analysis. *Zoologichesky Zhurnal* 90 (4): 402–411. [In Russian.]

Kotov A.A., Karabanov D.P., Bekker E.I., Neretina T.V. & Taylor D.J. 2016. Phylogeography of the *Chydorus sphaericus* group (Cladocera: Chydoridae) in the Northern Palearctic. *PLoS ONE* 11 (12): e0168711. https://doi.org/10.1371/journal.pone.0168711

Kotov A.A., Garibian P.G., Bekker E.I., Taylor D.J. & Karabanov D.P. 2021. A new species group from the *Daphnia curvirostris* species complex (Cladocera: Anomopoda) from the eastern Palaearctic: taxonomy, phylogeny and phylogeography. *Zoological Journal of the Linnean Society* 191 (3): 772–822. https://doi.org/10.1093/zoolinnean/zlaa046

Leigh J.W., Bryant D. & Nakagawa S. 2015. POPART: full-feature software for haplotype network construction. *Methods in Ecology & Evolution* 6 (9): 1110–1116. https://doi.org/10.1111/2041-210X.12410

Lilljeborg W. 1900. Cladocera Sueciae. *Nova acta regiae societatis scientiarum upsaleinsis, seriei tertiae* 19: 1–701.

Manuilova E.F. 1964. *Water Fleas (Cladocera) of USSR Fauna*. Nauka, Leningrad. [In Russian.]

Margaritora F.G. 1985. *Cladocera. Fauna d'Italia, Vol. 23*. Editioni Caldernini, Bologna.

Martínez-Caballero A.L., Morales-Gutiérrez S. & Elías-Gutiérrez M. 2017. First record of the genus *Bunops* Birge, 1893 (Cladocera: Macrothricidae) in the Neotropical highlands of Mexico with a detailed study of morphology and DNA barcodes. *Zootaxa* 4300 (4): 589–600. https://doi.org/10.11646/zootaxa.4300.4.7

Meng G., Li Y., Yang C. & Liu S. 2019. MitoZ: a toolkit for animal mitochondrial genome assembly, annotation and visualization. *Nucleic Acids Research* 47(11): e63. https://doi.org/10.1093/nar/gkz173

Müller P.E. 1867. Danmarks Cladocera. *Naturhistorisk tidsskrift* 3: 53–240.

Neretina A.N. & Kotov A.A. 2017. Diversity and distribution of the *Macrothrix paulensis* species group (Crustacea: Cladocera: Macrothricidae) in the tropics: what can we learn from the morphological data? *Annales de Limnologie-International Journal of Limnology* 53: 425–465. https://doi.org/10.1051/limn/2017022

Nilssen J.P., Hobæk A., Petrusek A. & Skage M. 2007. Restoring *Daphnia lacustris* G.O. Sars, 1862 (Crustacea, Anomopoda): a cryptic species in the *Daphnia longispina* group. *Hydrobiologia* 594: 5–17. https://doi.org/10.1007/s10750-007-9076-3

Norman A.M. & Brady G.S. 1867. A monograph of the British Entomostraca belonging to the families Bosminidae, Macrothricidae and Lynceidae. *Natural history transactions of Northumberland and Durham* 1 (3): 1–57.

Novichkova A.A. & Chertoprud E.S. 2015. The freshwater crustaceans (Cladocera: Copepoda) of Bering Island (Commander Islands, Russian Far East): species richness and taxocene structure. *Journal of natural History* 50 (21–22): 1357–1368. https://doi.org/10.1080/00222933.2015.1113319

Octorina P., Böhm A., Martin-Creuzburg D. & Straile D. 2022. Morphological defences and defence–cost trade-offs in *Daphnia* in response to two co-occurring invertebrate predators. *Freshwater Biology* 67 (5): 883–892. https://doi.org/10.1111/fwb.13888

Okonechnikov K., Golosova O., Fursov M. & the UGENE team. 2012. Unipro UGENE: a unified bioinformatics toolkit. *Bioinformatics* 28: 1166–1167. https://doi.org/10.1093/bioinformatics/bts091

Parenzan P. 1932. Cladocera. Sistematica e corologia dei Cladoceri limnicoli italiani ed appendice sui Cladoceri in generale. *Bolletino di Pesca, Piscicoltura e di Idrobiologia* Suppl. 8B: 1–340.

Pereboev D.D., Garibian P.G., Karabanov D.P., Efeykin B.D., Galimov Y.R., Petrusek A. & Kotov A.A. 2025. A non-monophyly of 'crowned' *Daphnia* (*Ctenodaphnia*) Dybowski et Grochowski, 1895 (Cladocera: Daphniidae): from genomes to morphology. *Zoologica Scripta* 54 (1): 69–90. https://doi.org/10.1111/zsc.12695

QGIS Development Team. 2026. QGIS Geographic Information System. QGIS Association, USA. Available from https://qgis.org [accessed 27 Aug. 2026].

Quirino B.A., Teixeira de Mello F., Deosti S., Bonecker C.C., Cardozo A.L.P., Yofukuji K.Y., Aleixo M.H.F. & Fugi R. 2021. Interactions between a planktivorous fish and planktonic microcrustaceans mediated by the biomass of aquatic macrophytes. *Journal of Plankton Research* 43 (1): 46–60. https://doi.org/10.1093/plankt/fbaa061

Righetti N., Nicolini F., Forni G. & Luchetti A. 2025. Towards a time-tree solution for Branchiopoda diversification: a jackknife assessment of fossil age priors. *Palaeoentomology* 8 (3): 316–328. https://doi.org/10.11646/palaeoentomology.8.3.8

Rogers D.C., Kotov A.A., Sinev A.Y., Glagolev S.M., Korovchinsky N.M., Smirnov N.N. & Bekker E.I. 2019. Arthropoda: Class Branchiopoda. *In*: Rogers D.C. & Thorp J.H. (eds) *Thorp and Covich's Freshwater Invertebrates*: 643–724. Academic Press, Elsevier, London, San-Diego, Cambridge, Kidlington. https://doi.org/10.1016/B978-0-12-385024-9.00018-6

Sars G.O. 1862a. Meddeelte en af talrige Afbildlinger ledsaget Oversight af de ar ham i Omegmen af Christiania iagtagne Crustacea Cladocera. *Forhandlinger Videnskabs-Selskabet Christiania aar 1861*: 144–167.

Sars G.O. 1862b. Fortsatte sit Foredrag over de af ham i Omegmen af Christiania iagttagne Crustacea. *Forhandlinger Videnskabs-Selbkabet Christiania aar 1861*: 250–302.

Sayers E.W., Cavanaugh M., Clark K., Ostell J., Pruitt K.D. & Karsch-Mizrachi I. 2019. GenBank. *Nucleic Acids Research* 47 (D1): D94–D99. https://doi.org/10.1093/nar/gky989

Scourfield D.J. & Harding J.P. 1966. *A Key to the British freshwater Cladocera*. *Scientific Publication, Vol. 5, 3rd Edition*. Freshwater Biological Association, Ambleside.

Schneider C., Rasband W. & Eliceiri K. 2012. NIH Image to ImageJ: 25 years of image analysis. *Nature Methods* 9: 671–675. https://doi.org/10.1038/nmeth.2089

Silva-Briano M. & Dumont H.J. 2001. *Wlassicsia*, *Bunops* and *Onchobunops* (Anomopoda), three related genera. *Hydrobiologia* 442: 1–28. https://doi.org/10.1023/A:1017502703931

Sinev A.Y., Karabanov D.P. & Kotov A.A. 2020. A new North Eurasian species of the *Alona affinis* complex (Cladocera: Chydoridae). *Zootaxa* 4767 (1): 115–137. https://doi.org/10.11646/zootaxa.4767.1.5

Smirnov N.N. 1976. *Macrothricidae and Moinidae of the World Fauna.* Fauna SSSR, novaya seriya, Rakoobraznye 1(3). Nauka, Leningrad. [In Russian.]

Smirnov N.N. 1992. *The Macrothricidae of the World. Guides to the Identification of the Microinvertebrates of the Continental Waters of the World, Vol 1*. SPB Academic Publishing, The Hague.

Smith D.G. 2001. Cladoceran Branchiopoda (Water fleas). *In*: Smith D.G. (ed.) *Pennak's Freshwater Invertebrates of the United States, 4th edition*: 453–488. Wiley, New York.

Sperfeld E., Nilssen J.P., Rinehart S., Schwenk K. & Hessen D.O. 2020. Ecology of predator-induced morphological defense traits in *Daphnia longispina* (Cladocera, Arthropoda). *Oecologia* 192 (3): 687–698. https://doi.org/10.1007/s00442-019-04588-6

Sramek-Hušek R., Straskraba M. & Brtek J. 1962. *Lupenonozci–Branchiopoda. Fauna CSSR. Svazek, v. 16*. Nakladatelstvi Československé Academie Věd, Praha. [In Czech.]

Streletskaya E.A. 2010. A review of wheel bearer (Rotifera), water flea (Cladocera) and copepod (Copepoda) fauna of the Anadyr River basin. *Sibirskii Ekologicheskii Zhurnal* 17(4): 649–662. [In Russian.]

Uéno M. 1932. Die Süßwasser-Branchiopoden der Nord-Kurilen. *Internationale Revue der gesamten Hydrobiologie und Hydrographie* 27 (1–3): 102–104. https://doi.org/10.1002/iroh.19320270103

Van Damme K. & Dumont H.J. 2006. Sex in a cyclical parthenogen: mating behaviour of *Chydorus sphaericus* (Crustacea; Branchiopoda; Anomopoda). *Freshwater Biology* 51 (12): 2334–2346. https://doi.org/10.1111/j.1365-2427.2006.01654.x

Van Damme K., Cornetti L., Fields P.D. & Ebert D. 2022. Whole-genome phylogenetic reconstruction as a powerful tool to reveal homoplasy and ancient rapid radiation in waterflea evolution. *Systematic Biology* 71 (4): 777–787. https://doi.org/10.1093/sysbio/syab094

Wong T.K., Ly-Trong N., Ren H., Baños H., Roger A.J., Susko E., ... & Minh B.Q. 2026. IQTREE3: phylogenomic inference software using complex evolutionary models. *Molecular Biology and Evolution* 43 (5): msag117. https://doi.org/10.1093/molbev/msag117

Xu S.L., Han B.P., Martínez A., Schwentner M., Fontaneto D., Dumont H.J. & Kotov A.A. 2021. Mitogenomics of Cladocera (Branchiopoda): Marked gene order rearrangements and independent predation roots. *Molecular Phylogenetics and Evolution* 164: e107275. https://doi.org/10.1016/j.ympev.2021.107275

Yermolayeva N.I & Fetter G.V. 2020. A record of *Drepanothrix dentata* (Eurén, 1861) (Cladocera, Macrothricidae) in small lakes of South Baikalia. *Zoologicheskiy Zhurnal* 99 (4): 475–478. [In Russian.] https://doi.org/10.31857/S0044513420040078

Zuykova E.I., Bochkarev N.A., Taylor D.J. & Kotov A.A. 2019. Unexpected endemism in the *Daphnia longispina* complex (Crustacea: Cladocera) in Southern Siberia. *PloS ONE* 14 (9): e0221527. https://doi.org/10.1371/journal.pone.0221527

Printed versions of all papers are deposited in the libraries of two of the institutes that are members of the *EJT* consortium: Muséum national d'Histoire naturelle, Paris, France and Royal Museum for Central Africa, Tervuren, Belgium. The other members of the consortium are: Royal Belgian Institute of Natural Sciences, Brussels, Belgium; Meise Botanic Garden, Meise, Belgium; Natural History Museum of Denmark, Copenhagen, Denmark; Naturalis Biodiversity Center, Leiden, the Netherlands; Museo Nacional de Ciencias Naturales-CSIC, Madrid, Spain; Leibniz Institute for the Analysis of Biodiversity Change, Bonn – Hamburg, Germany; National Museum of the Czech Republic, Prague, Czech Republic; The Steinhardt Museum of Natural History, Tel Aviv, Israël.

Supplementary files

Supp. file 1. Fig. S1. Midpoint-rooted maximum likelihood phylograms based on individual barcoding markers. **A**. Folmer's *COI* gene fragment. **B**. *16S rRNA* gene. **C**. ITS1. The node support values are based on SH-aLRT/ultrafast bootstrap. Colours indicate major phylogroups.
https://doi.org/10.5852/ejt.2026.1090.3321.14584

Supp. file 2. Supplementary tables. https://doi.org/10.5852/ejt.2026.1090.3321.14585

Supp. file 3. Alignment of the mitochondrial interribosomal region of *Drepanothrix* dentata from Lake Glubokoe, Moscow Region, Russia (IEE AAK M–7018): a sequence extracted from mitogenome assembly against an independently sequenced fragment amplified by PCR.
https://doi.org/10.5852/ejt.2026.1090.3321.14586